Icarus 211 (2011) 1215–1232

Contents lists available at ScienceDirect

Icarus

journal homepage: www.elsevier.com/locate/icarus

Changes in Jupiter's zonal velocity between 1979 and 2008 ☆

Xylar S. Asay-Davis [a,*], Philip S. Marcus [b], Michael H. Wong [c], Imke de Pater [c]

[a] Center for Nonlinear Studies, Los Alamos National Laboratory, Los Alamos, NM 87545, United States
[b] Department of Mechanical Engineering, University of California, Berkeley, CA 94720, United States
[c] Department of Astronomy, University of California, Berkeley, CA 94720, United States

ARTICLE INFO

Article history:
Received 30 March 2010
Revised 18 October 2010
Accepted 13 November 2010
Available online 21 November 2010

Keywords:
Jupiter, Atmosphere
Atmospheres, Dynamics
Atmospheres, Evolution

ABSTRACT

We show that the peak velocity of Jupiter's visible-cloud-level zonal winds near 24°N (planetographic) increased from 2000 to 2008. This increase was the only change in the zonal velocity from 2000 to 2008 for latitudes between ±70° that was statistically significant and not obviously associated with visible weather. We present the first automated retrieval of fast (∼130 m s^{-1}) zonal velocities at 8°N planetographic latitude, and show that some previous retrievals incorrectly found slower zonal winds because the eastward drift of the dark projections (associated with 5-μm hot spots) "fooled" the retrieval algorithms.

We determined the zonal velocity in 2000 from Cassini images from NASA's Planetary Data System using a *global* method similar to previous longitude-shifting correlation methods used by others, and a new *local* method based on the longitudinal average of the two-dimensional velocity field. We obtained *global* velocities from images acquired in May 2008 with the Wide Field Planetary Camera 2 (WFPC2) on the Hubble Space Telescope (HST). Longer-term variability of the zonal winds is based on comparisons with published velocities based on 1979 Voyager 2 and 1995–1998 HST images. Fluctuations in the zonal wind speeds on the order of 10 m s^{-1} on timescales ranging from weeks to months were found in the 1979 Voyager 2 and the 1995–1998 HST velocities. In data separated by 10 h, we find that the east–west velocity uncertainty due to longitudinal fluctuations are nearly 10 m s^{-1}, so velocity fluctuations of 10 m s^{-1} may occur on timescales that are even smaller than 10 h. Fluctuations across such a wide range of timescales limit the accuracy of zonal wind measurements. The concept of an average zonal velocity may be ill-posed, and defining a "temporal mean" zonal velocity as the average of several zonal velocity fields spanning months or years may not be physically meaningful.

At 8°N, we use our *global* method to find peak zonal velocities of ∼110 m s^{-1} in 2000 and ∼130 m s^{-1} in 2008. Zonal velocities from 2000 Cassini data produced by our *local* and *global* methods agree everywhere, except in the vicinity of 8°N. There, the *local* algorithm shows that the east–west velocity has large variations in longitude; vast regions exceed ∼140 m s^{-1}. Our *global* algorithm, and all of the velocity-extraction algorithms used in previously-published studies, found the east–west drift velocities of the visible dark projections, rather than the true zonal velocity at the visible-cloud level. Therefore, the apparent increase in zonal winds between 2000 and 2008 at 8°N is not a true change in zonal velocity.

At 7.3°N, the Galileo probe found zonal velocities of 170 m s^{-1} at the 3-bar level. If the true zonal velocity at the visible-cloud level at this latitude is ∼140 m s^{-1} rather than ∼105 m s^{-1}, then the vertical zonal wind shear is much less than the currently accepted value.

Published by Elsevier Inc.

1. Introduction

One of the most robust features of Jupiter's weather layer is its zonal velocity. Here, we define the "zonal flow" to be the axisymmetric component, or longitudinal average of the east–west component of the winds in the visible-cloud deck. The zonal velocity of Jupiter's winds is a strong, and oscillatory, function of latitude, but it also varied significantly in elevation in the one time and place in which that variation was measured directly (Atkinson et al., 1998) and also changes weakly in time. Between 1979 and 2000, several published zonal velocities (as functions of latitude) were extracted from spacecraft images, showing that the zonal velocity, which has characteristic velocities of order 100 m s^{-1}, had temporal variability on the order of 10 m s^{-1} at most latitudes.

Historically, there have been two general ways of measuring Jupiter's zonal flow. In one way (the most common), which we refer to here as a *global* method, the zonal velocity is computed directly from image or mosaic pairs without having to first find the

☆ Partly based on observations obtained from the data archive at the Space Telescope Science Institute. STScI is operated by the Association of Universities for Research in Astronomy, Inc. under NASA Contract NAS 5-26555.

* Corresponding author.
E-mail address: xylar@lanl.gov (X.S. Asay-Davis).

0019-1035/$ - see front matter Published by Elsevier Inc.
doi:10.1016/j.icarus.2010.11.018

individual two-dimensional velocity vectors that make up the velocity fields. Rather, the zonal flow is computed by finding longitudinal correlations of the clouds in the region of an image or mosaic pair that span a very large range in longitude (often the entire circumference of the planet) and a very small range in latitude (Limaye, 1986, 1989; García-Melendo and Sánchez-Lavega, 2001; Porco et al., 2003).

Global methods typically use computer-automated algorithms to find the correlations, and because the correlation is done over a large range in longitude, no information is available about how the east–west component of the velocity varies in longitude. In addition, because the correlations are found with respect to displacements in longitude but not latitude, there is no information available about the magnitude of the north–south components of the velocity with respect to the east–west components.

A global method for computing a "zonal flow" is guaranteed to find a single value for the zonal velocity at a given latitude, regardless of longitudinal variability. The resulting zonal flow can be misleading. For example, in Neptune's weather layer, at many latitudes the variations of the east–west component of the velocity as a function of longitude are of the same order as the east–west velocity itself (Smith et al., 1989; Limaye and Sromovsky, 1991; Martin et al., 2004). A "zonal flow" of Neptune showing a smooth sinusoidal variation in latitude can be extracted with a global method, but it is not clear how to interpret that flow. In what sense is the dominant atmospheric flow on Neptune zonal? On Jupiter, with the exception of the flows within compact vortices or near the poles, the longitudinal variations of the east–west component of the velocity are much smaller than the characteristic magnitude of the east–west velocity. In addition, with the exception of the flows in the compact, intense vortices, the north–south component of the jovian velocities are much smaller than the east–west components. Thus, it is clear that it makes sense to say that the jovian atmosphere has a dominant zonal flow and to compute it with a global method.

However, it is still possible that the extracted "zonal flow" is misleading, as shown by a second class of methods, which we call *local* methods, for computing a zonal flow. In general, unless a planet's atmospheric flow is *exactly* axisymmetric, local and global methods will give different results for the "zonal flow." In a local method, the first step is to compute the individual, two-dimensional velocity vectors that make up the velocity field. The vectors are computed using correlations or tie points between a pair of images or mosaics using information that is local to the position of the velocity vector. The zonal flow is then computed by averaging the east–west components of the vectors over longitude and/or time (Ingersoll et al., 1981; Limaye et al., 1982; Li et al., 2004, 2006)[1] In all previously-published studies, the velocity vectors used to compute the zonal flow with a local method were extracted with manual feature tracking rather than using an automated correlation method. Asay-Davis et al. (2009) argued that the uncertainty of a velocity vector computed manually may be greater than the uncertainty computed with an automated method; the main difficulty of manual methods of velocity extraction is that, over a specified spatial region, they typically extract 100–1000 times fewer velocities than does an automated method (cf., compare Figs. 1 and 3 in Shetty and Marcus (2010), and the two panels of Fig. 2 in Asay-Davis et al. (2009)). Thus, although computing the zonal velocity with a local method is possible using a manual method to extract the velocity vectors, there are typically an insufficient number of velocity vectors to compute a statistically meaningful variation in the velocity field as a function of longitude. On the other hand, a local method in which the velocity vectors have been computed with an automated technique will, as we show below, have sufficient information to determine the longitudinal variability of the east–west flows.

Historically, the uncertainties of the published zonal velocities were based on the temporal fluctuations of the zonal velocities, although the uncertainties were not always published (Porco et al., 2003). In general, when several different, independent zonal velocities were obtained from images or mosaics that spanned a short interval of time, the reported uncertainties of the zonal velocities were defined to be the RMS temporal variation of the zonal velocities (Limaye, 1986, 1989; García-Melendo and Sánchez-Lavega, 2001). These uncertainties are attributable to both random errors and the true temporal variations of the zonal flow, including temporal variations of the east–west flow's variations in longitude. Understanding these uncertainties is important if we want to understand how the jovian zonal velocity has evolved over time. We cannot claim that a flow has changed in time if we cannot demonstrate that the change is greater than the uncertainty. Moreover, (Limaye, 1989) has argued that the jovian zonal flow has temporal variations on the timescales of days, weeks and months that are on the same order ($10\ m\ s^{-1}$) as the temporal variations that have been reported to occur on the decade timescale. Thus, what may have been reported as changes that occurred over decades may in fact be changes that occurred over weeks, but were merely sampled over decades. To clarify some of the issues associated with the temporal changes in zonal flows, we present here two new methods for computing the uncertainties of the zonal velocities: one for a global method and one for a local method. Neither method uses temporal variations.

In Section 2, we summarize the previous analyses of zonal flows. In Section 3, we present our Hubble Space Telescope (HST) observations from May 2008 from which we acquired a series of images covering two full jovian rotations using the Wide Field Planetary Camera 2 (WFPC2). We also explain our *global* method for extracting zonal velocities and their uncertainties. In Section 4, we compare our zonal velocity extracted from HST 2008 images to zonal velocities that we extract from earlier observations also using our global method. We also compare with zonal velocities computed by others using similar global methods. We examine changes in the zonal velocity that are greater than the measured uncertainties. In Section 5 we present the zonal velocity of 2000 and its uncertainties extracted with our local method and examine the large differences between the locally and globally-extracted velocities. We examine the relative sensitivities of these methods to the dark projections, at 8.2°N. In Section 6, we state our conclusions and plans for future work.

2. Summary of previously published zonal velocities

2.1. Wavelength of images and height of the extracted velocities

In this study, we explore temporal variability of Jupiter's zonal wind by comparing our extracted zonal velocities with three prior zonal velocity measurements. Previously, zonal velocities were extracted by numerous authors from Voyager 1 and 2 images from 1979 (see Section 1), by García-Melendo and Sánchez-Lavega (2001) from HST images from 1995–1998 and by Porco et al. (2003) and Li et al. (2006) from Cassini images from 2000. We use the results of Limaye (1986) for Voyager zonal winds because these were derived from the largest number of mosaics using an extraction method similar to our own and those of García-Melendo

[1] Li et al. (2004) call their "local" method a "feature tracking" method, and what we call a "global" method, they call a "correlation method". We use different terminology because their "feature tracking" method is slightly different than what we have defined as a "local" method. Instead of using the velocity vectors from all of their features, Li et al. select a subset of features in which they exclude many features based on their shape, their meridional velocity, and/or the temporal variability over 60 h.

and Sánchez-Lavega (2001) and Porco et al. (2003). We compared our results with the Cassini velocity measurements of Porco et al. (2003); this profile was constructed from the same images (though with slight differences in navigation, see Section 4.6) as we used to construct our Cassini zonal velocity profile. Table 1 shows the filters that were used in these images along with the filters of the HST images from 2008 that we use in our new extraction of the zonal winds reported here.

Limaye (1989) and García-Melendo and Sánchez-Lavega (2001), among others, compared zonal velocities extracted from images produced with filters at different wavelengths. Limaye (1989) found some differences between the Voyager zonal velocities produced from blue filter (480 nm) images vs. those from violet filter (400 nm) images, though even the largest of these differences appear to be of the same order as the temporal fluctuations in the zonal velocity over several tens of rotations. García-Melendo and Sánchez-Lavega (2001) saw no important difference between zonal velocities taken at 892, 410 and 953 nm. Zonal velocities from each of these wavelengths were averaged together to produce their mean zonal velocity for the period between 1995 and 1998.

Porco et al. (2005) found significant variation in the zonal velocity of Saturn at different wavelengths (which probe different depths). On Jupiter, Li et al. (2006) measured vertical wind shear above the visible-cloud deck by manually tracking features that appeared only in ultraviolet images. Li et al. (2006) also argued that they tracked features at 3 bar or deeper (below the main visible-cloud deck), by tracking (in the CB2 and MT2 filters at 750 and 727 nm, respectively) clouds within the dark projections, which are relatively cloudless regions in the weather layer and therefore are windows to the deeper layers. With this selective approach, Li et al. (2006) confirmed that zonal winds decay with height above the visible-cloud decks, consistent with Cassini CIRS thermal winds (Flasar et al., 2004), and also argued that they confirmed that zonal winds increased with depth near 7°N, consistent with the vertical wind shear measured by the Galileo Probe at 7.3°N (Atkinson et al., 1998). Conversely, the analysis of Li et al. (2006) shows that, with the possible exception of the flows at the dark projections, velocity extractions with images made with the visible wavelengths used in this study measure only the zonal velocities in the visible-cloud deck and do not measure velocities above them. Furthermore, the analysis implied that a necessary (but not sufficient) condition to measure velocities below the visible-cloud level using images in visible wavelengths is that there is a large "hole" in the visible-cloud deck, such as a hole associated with a dark projection. This means that, at least at the vast majority of latitudes on Jupiter where there are no large holes in the cloud deck, it is reasonable to intercompare zonal velocity profiles taken at different wavelengths to look for temporal variability.

Table 1
Wavelengths for the image filters used to produce each of the four zonal velocities analyzed in this paper. As discussed in Section 3.1, previous researchers have found that the zonal velocity does not vary significantly over the depths probed by these wavelengths, suggesting that zonal velocities constructed from images at different wavelengths can be reasonably compared with one another. Also listed are the approximate resolution of the original images before deprojection (after deprojection in the case of Voyager).

Data set	Filter wavelengths (nm)	Sub-observer resolution (km pixel^{-1})
HST 2008	673	155
Cassini 2000	750 (CB2)	125
HST 1995–1998	410, 892, 953	140–190
Voyager 2 1979	400	138*

* Resolution of map mosaics used.

2.2. Uncertainty quantification in previous work

One of the difficulties in distinguishing real temporal variation in the mean zonal velocity from errors in the measurements is that the zonal velocity appears to vary on a variety of timescales from weeks to decades (and quite probably over shorter and longer times that have not yet been reliably measured). Because measurements have been taken only sporadically, it is sometimes impossible to know when a change occurred and how long it took to occur. Limaye (1986, 1989) performed a particularly detailed analysis of mosaics covering several hundred jovian rotations from the Voyager 1 and Voyager 2 approaches. At each latitude bin, two mean zonal velocities were constructed by averaging all of the zonal velocities at that latitude from each spacecraft. At some latitudes, Limaye (1989) found differences in the mean zonal velocities of more than 10 m s^{-1} over the four month interval between Voyagers 1 and 2. He saw variability of approximately the same magnitude within a period of 10–50 jovian rotations (a few weeks). In fact, fluctuations of more than 7 m s^{-1} were typically seen between velocities extracted from consecutive rotations; Limaye speculated that at least some of this variability was due to real temporal variation in the mean zonal velocity, as opposed to errors in the extraction method. The zonal velocities of García-Melendo and Sánchez-Lavega (2001) taken between 1995 and 1998 show changes at several latitudes on the order of 10–15 m s^{-1} from one year to the next. Taken together, these studies suggest that it is difficult to distinguish between changes that occurred over months from those that occurred over years, and that both of these longer-term changes are hard to distinguish from the fluctuations (whether real or errors) that occur in a single rotation.

Some previous methods for measuring the uncertainties in the mean zonal velocity have assumed that the variability among a large number of zonal velocities is due to the errors in the extraction method and to the random fluctuations in the velocity field over short timescales. These errors and fluctuations were assumed to be random or uncorrelated, so that if there were no long-term changes in the zonal velocity, then at each latitude bin, the average of N zonal velocities at that latitude would produce a mean zonal velocity with uncertainties that are smaller than the uncertainty of an individual zonal velocity and also smaller than the variations between pairs of zonal velocities by a factor of $\sqrt{N}$. In particular, the Voyager 2 1979 (Limaye, 1986) zonal velocity has uncertainties that were based on the root-mean-squared (RMS) deviation of the fluctuations of all zonal velocities from the mean zonal velocity, divided by $\sqrt{N}$. The mean zonal velocity $\bar{v}(\theta)$ and its RMS deviation $RMS(\theta)$ as a function of latitude θ were defined:

$$\bar{v}(\theta) \equiv \frac{1}{N}\sum_i v_i(\theta) \tag{1}$$

$$RMS(\theta) \equiv \sqrt{\frac{\sum_i [v_i(\theta) - \bar{v}(\theta)]^2}{N}} \tag{2}$$

where the sum is over the available zonal velocities. The mean zonal velocity and its RMS deviation in Limaye (1986) were constructed in this manner in each latitude bin from from 142 zonal velocities, and the uncertainty in the mean zonal velocity was defined to be $RMS/\sqrt{N}$. However, there is a question of whether $RMS/\sqrt{N}$ is a meaningful uncertainty for the Voyager zonal velocities. The use of $RMS/\sqrt{N}$ as a measure of the uncertainties is only appropriate if the changes in the "true" mean zonal velocity are small compared with this measure of the uncertainties. Limaye (1989) and García-Melendo and Sánchez-Lavega (2001) present evidence of changes on timescales of months or years in the mean zonal velocity that are larger than their uncertainties. These temporal changes contribute substantially to the uncertainty in a time-averaged zonal

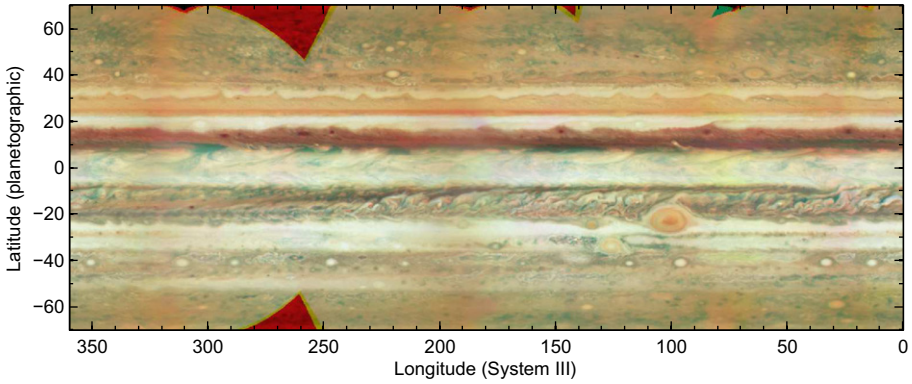

Fig. 1. A color HST mosaic taken with 673 nm (red), 502 nm (green) and 410 nm (blue) filters on May 10, 2008. In some regions (those with dark red color), only images in at 673 nm were available. Only the 673 nm images were used to produce the HST 2008 zonal velocity.

velocity computed from individual zonal velocities that span months or years. Such a time-averaged zonal velocity will have an uncertainty that is much larger that $RMS/\sqrt{N}$ because of these changes, so that a more conservative estimate of the magnitude of uncertainty in the zonal velocities during the Voyager 2 approach is its RMS deviation $RMS_{Voyager2}$ (without dividing by $\sqrt{N}$). We define $RMS_{Voyager2}$ to be the published RMS deviation in Limaye (1986), which is $\sqrt{N} \sim \sqrt{142}$ times greater than Limaye's published error uncertainty. (Not all zonal velocities are available at all latitudes, so that N varies slightly with latitude.) Similarly, we define $RMS_{HST95-98}$ as the temporal RMS of the HST zonal velocities between 1995 and 1998 as determined by García-Melendo and Sánchez-Lavega (2001), as they did, without division by $\sqrt{N}$.

3. Observations and analysis: May 2008 HST and December 2000 Cassini images

3.1. Deprojection and navigation

We used HST images taken with the WFPC2 on UT May 9 and 10, 2008 to construct our zonal velocities (see Appendix A for the identifiers corresponding to these images). The pixel resolution of the images at the jovian disk center is ~155 km pixel^{-1}. We acquired a majority of the images in this data set with the F673N filter (673 nm). A similar wavelength had provided the highest contrast among cloud features in the vicinities of the Great Red Spot (GRS) and Oval BA (Asay-Davis et al., 2009). Since cloud features can only be tracked between images taken at the same wavelength, we were able to maximize the number of image pairs from which we could extract velocity measurements by focusing mostly on a single wavelength. The large number of measurements can be used to reduce the influence of bad pixels and Poissonian shot noise on the extracted zonal velocity.

The HST images were navigated and deprojected using the same methods outlined in Asay-Davis et al. (2009) and Lii et al. (2010). Images were deprojected onto a regular grid in planetographic latitude and System-III longitude with 0.05° spacing, sub-sampling the original imaging data at ~55–60 km pixel^{-1} at disk center. Fig. 1 shows a mosaic of Jupiter at all longitudes and from 70°N to 70°S latitude constructed from our HST images. Reflectivity data were divided by the cosine of the emission angle to remove the first order illumination effect from the maps.

We used 75 Cassini image maps from December 11 to 13, 2000 (see Appendix A for the identifiers corresponding to these images). These image maps were provided by Ashwin Vasavada, who processed these images as described in Porco et al. (2003) and Vasavada et al. (2006). The Cassini maps, and the description of their processing, are available through the Atmospheres Node of the Planetary Data System (PDS).[2] The deprojection grid has a fixed spacing in *planetocentric* latitude and System-III longitude of 0.1° spacing, corresponding to ~110–120 km pixel^{-1} at the disk center.

3.2. Global method for extracting the zonal velocity

Rather than producing a zonal velocity from mosaics, we work with deprojected image pairs directly. Our approach has at least two advantages. First, the time separation between our HST image pairs varies considerably, from about 9 h to about 11 h. This variability would make construction of useful mosaics difficult, since a mosaic pair is assumed to have a fixed time separation. Second, a mosaic can only make use of one image (or a linear combination of images) at a given longitude, whereas we extract useful correlation data from all images that cover a given longitude. This redundancy tends to reduce errors due to bad pixels, Poissonian shot noise, or random navigational offsets (though not systematic navigation errors).

We crop each image to within ±40° longitude of the central meridian to avoid correlating parts of the image where cloud features are obscured by haze. Correlations are performed between all overlapping image pairs separated by approximately one jovian rotation. At each planetographic latitude θ, we search a range of possible velocities $v(\theta)$ that is within ±50 m s^{-1} of the most recent published zonal velocity of Porco et al. (2003). For the image pair consisting of the jth and kth images in the data set (I_j, I_k), at each latitude and for each possible velocity v, we compute:

$$\Delta\phi_{j,k}(v) \equiv v\Delta t_{j,k}\frac{d\phi}{dx} \tag{3}$$

$$\frac{dx}{d\phi} = \frac{R_E\cos\theta}{\sqrt{1-e^2\sin^2\theta}} \tag{4}$$

$$e^2 = \frac{R_E^2 - R_P^2}{R_E^2} \tag{5}$$

where $\Delta\phi_{j,k}$ is the shift in longitude corresponding to a given v for the image pair, $\Delta t_{j,k}$ is the time separating the pair of images, R_E and R_P are Jupiter's equatorial and polar radii (71,492 km and 66,854 km, respectively, the IAU standard 1-bar radii from Seidelmann et al. (2007)), and e is the eccentricity. Eqs. (4) and (5) are Eqs. (19) and (2) from Ch. 3 of Pearson (1990). Correlations are made between an image I_j and a shifted image I'_k, where the second image has been shifted in longitude by $\Delta\phi_{j,k}(v)$, so that

$$I'_k(\theta,\phi) \equiv I_k(\theta, \phi + \Delta\phi_{j,k}(v)) \tag{6}$$

[2] http://pds-atmospheres.nmsu.edu/Jupiter/jupiter.html.

Values of I'_k are found by cubic interpolation in the longitude direction of I_k. We define the cross correlation of the unshifted image I_j with the shifted image I'_k as

$$\langle I_j I'_k \rangle(\theta, v) \equiv \frac{1}{N_{j,k}} \sum_{i=1}^{N_{j,k}} I_j(\theta, \phi_i) I'_k(\theta, \phi_i) \tag{7}$$

where $N_{j,k}$ is the number of overlapping pixels between the images for a given θ and v, and where ϕ_i is the longitude of the ith pixel. The mean and variance of an image can be defined in a manner consistent with (7) as

$$\langle I_j \rangle(\theta, v) \equiv \frac{1}{N_{j,k}} \sum_{i=1}^{N_{j,k}} I_j(\theta, \phi_i) \tag{8}$$

$$\langle I_j^2 \rangle(\theta, v) \equiv \frac{1}{N_{j,k}} \sum_{i=1}^{N_{j,k}} I_j^2(\theta, \phi_i) \tag{9}$$

For each latitude theta, we determine the zonal velocity v that maximizes our correlation function,

$$R(\theta, v) = \sum_{(I_j, I_k)} \sum_{\theta'=\theta-\Delta\theta}^{\theta+\Delta\theta} \left[\frac{\langle I_j I'_k \rangle - N_{j,k} \langle I_j \rangle \langle I'_k \rangle}{\sqrt{\left(\langle I_j^2 \rangle - N_{j,k} \langle I_j \rangle^2 \right) \left(\langle I_k'^2 \rangle - N_{j,k} \langle I'_k \rangle^2 \right)}} \right] \tag{10}$$

where each bracketed quantity is evaluated at (θ', v), where the first sum is over all overlapping image pairs (I_j, I_k) and where the second sum is over all latitudes within $\pm\Delta\theta$ of the given latitude θ. For our HST 2008 zonal velocity, $\Delta\theta = 0.25°$, and for our Cassini 2000 zonal velocity, $\Delta\theta = 0.5°$, meaning that correlations were found over five rows of pixels on either side of the latitude of interest in both cases (11 rows in total). Correlating more than one row of pixels at a time (i.e., having $\Delta\theta > 0$) tends to remove spurious correlations caused by coherent structures. We found that $\Delta\theta$ equal to five rows of pixels was sufficient to remove the worst spurious features without smoothing robust peaks (as a function of latitude) in the zonal velocity. The latitude spacing of a zonal velocity was the same as that of the images (i.e., there is a value of the zonal velocity to correspond to each row of pixels). This means that zonal velocity values that are adjacent in latitude were produced using many of the same image pixels.

The definition of the correlation function in (10) was taken from the laboratory correlation technique Correlation Image Velocimetry (CIV) (Fincham and Spedding, 1997; Fincham and Delerce, 2000). The normalization factors in the denominator remove changes in overall contrast between images, while subtraction of the second term in the numerator removes variations in overall brightness between images. García-Melendo and Sánchez-Lavega (2001) used a correlation function that was the cross correlation of the image pairs without the normalization factors, and with the average brightness removed using a high-pass filter method (García-Melendo et al., 2000). Limaye (1986, 1989) found correlations by minimizing the least cumulative absolute difference between mosaics at a given latitude and summed over longitude. Limaye (1986) tested several definitions of the correlation function and found that there were negligible changes in the resulting zonal velocities for different correlation functions. We tested several alternative definitions of R (with and without normalization) including the cumulative absolute difference and found that R as defined in Eq. (10) peaked the most sharply with longitude offset. However, we did not see any appreciable difference in the resulting zonal velocity. Therefore, we feel confident that the choice of correlation technique is not contributing to the differences between the zonal velocities that we compare in this work.

3.3. Method for computing uncertainties with the global method

Our HST 2008 image data set contains only two jovian rotations. Therefore, we were able to construct only one zonal velocity as a function of latitude from these images. Our Cassini 2000 zonal velocity was constructed from images from four jovian rotations, so that each latitude bin is the average of three independent zonal velocities separated by 10 h. In neither case did we have enough independent zonal velocities to obtain meaningful statistics to determine the RMS deviation around a mean zonal velocity. Instead, for these two zonal velocities we made use of the *correlation velocity uncertainty* defined in Asay-Davis et al. (2009). A major advantage of the correlation velocity uncertainty is that it empirically derives uncertainties from the image and velocity field data themselves.

To determine the *correlation velocity uncertainty*, first, we used the newly extracted zonal velocity $v(\theta)$ to advect the pixels of each image to a common time (usually about halfway between the earliest and latest images). Unlike in Asay-Davis et al. (2009), we did not need to solve a 2D advection equation. Because the velocity was constant along each path and because the path was 1D, the advection could be accomplished using a simple shift in longitude. Since the longitudinal shift did not, in general, correspond to an integer number of pixels, we used cubic interpolation to construct the advected images from the originals. Second, we applied CIV, the laboratory velocity measurement technique mentioned in Section 3.2, to all overlapping pairs of the *advected* images. Although CIV was designed to find velocities, at a basic level it is a software for finding correlations among patterns of pixels; we used CIV to find displacements (rather than velocities) of cloud features between the advected images. The local *correlation velocity uncertainty* is the displacement between the *advected* cloud features divided by the true time separation for that pair of features, the time interval between the original, unadvected images. The uncertainty in the zonal velocity at a given latitude is the RMS value of all local *correlation velocity uncertainties* within a given range of that latitude (for all longitudes). We choose to use the same range of latitudes $\Delta\theta$ as appears in the correlation function in Section 3.2 (i.e., ±0.25° for the HST data, ±0.5° for the Cassini data).

Applying CIV to the full set of images proved to be time consuming. Computing a total of ~30,000,000 correlations between a subset of approximately 50% of the Cassini images took more than a month on a four processor desktop computer. To save computational time, we processed only 10% of the HST image pairs, producing ~1,200,000 correlations, which were used to compute the correlation uncertainty. (Although the software *attempted* to correlate a similar number of features in the Cassini and HST cases, the HST images contained visibly more noise than the Cassini images, resulting in far more spurious correlations between HST images. These spurious correlations were removed automatically by the CIV software using well established techniques (Fincham and Delerce, 2000).) The image pairs were chosen at random so as not to favor any range of longitudes. The resulting HST and Cassini uncertainties are quite similar: the RMS value of the *correlation velocity uncertainty* over all latitudes is 11.2 m s^{-1} for the HST data and 11.4 m s^{-1} for the Cassini data. The similarity suggests that we have taken a large enough sample of the HST images to get meaningful statistics.

3.4. Navigation errors

Limaye (1989) discussed in detail the navigational differences between the Voyager 1 and Voyager 2 mosaics that led to a latitudinal shift of approximately 0.5° between the mean zonal velocities extracted from these data. Limaye shifted each Voyager 1 zonal velocity north or south a (possibly non-integer) number of

mosaic pixels. (The mosaic pixels were apparently not equally spaced in latitude, so that the offset was not a constant latitude.) He used a correlation method to find the pixel shift that maximized the correlation between each Voyager 1 zonal velocity and the Voyager 2 mean zonal velocity. The relative latitude offset is assumed to be a relative navigation error between the Voyager 1 mosaic and the Voyager 2 mean. Relative navigation errors as large as ~0.4° latitude (about four pixels) were detected in this way. The average navigation error was ~0.15° latitude.

Visual comparison of our HST 2008 zonal velocity with both our Cassini 2000 zonal velocity and the HST 1995–1998 zonal velocity of García-Melendo and Sánchez-Lavega (2001) showed relative navigation errors between these image data sets that were similar to those between Voyager 1 and Voyager 2. It was visually apparent that these zonal velocities differed not only by latitudinal shifts but also by velocity offsets corresponding to a difference in rotating frame (i.e., a deviation from System-III rotation rate). (Note that a change in rotating frame corresponds to a velocity offset that varies with latitude, and is maximum at the equator.) To correct for the relative navigation errors, we assumed that our HST 2008 zonal velocity was correctly navigated and apply offsets to the other zonal velocities to match this "reference" zonal velocity.

We used a multidimensional minimization technique to find simultaneously the latitudinal offset and the velocity offset that produced the best match with the reference zonal velocity. The resulting offsets are catalogued in Table 2. Since the pixels in the HST 1995–1998 mosaics were equally spaced in planetographic latitude, we applied a constant offset in planetographic latitude to the HST 1995–1998 zonal velocity. Similarly, since the pixels of the Cassini 2000 images were at equally spaced intervals in planetocentric latitude, the Cassini 2000 zonal velocity was shifted by a constant planetocentric latitude. Because the Cassini 2000 images of the northern hemisphere had been navigated separately from those of the southern hemisphere, we computed latitudinal and velocity offsets separately for each hemisphere.

The latitudinal offsets in Table 2 for the HST and the Cassini zonal velocities are on the order of one pixel or smaller, suggesting that navigation methods may have uncertainties on the order of one pixel. The larger offset between the Voyager 2 and all other zonal velocities may be due to navigational errors or may result from true changes in the zonal velocity. In either case, a comparison of the shifted Voyager 2 zonal velocity gives the most conservative estimate of where changes greater than the uncertainties have occurred. The velocity offset values are negligible in the case of the Cassini 2000 data and small compared with the RMS fluctuations in the case of the Voyager 2 data, but significant in the case of the HST 1995–1998 data. For comparison, the difference between the equatorial velocity in Systems II and III is ~3.7 m s^{-1}. Although the System-III period has been revised by several researchers (Higgins et al., 2007; Russell et al., 2001), these changes are too small to be noticed in our analysis.

Table 2
Offsets in latitude and velocity applied to each zonal velocity in order to best match our HST 2008 zonal velocity, used as a reference. The velocity offsets are the values at the equator, where the value is maximum. The velocity offsets at other latitudes are modulated to correspond to the same rotating frame (i.e., the same offset in longitude per second). Latitude offsets for the Cassini zonal velocities are planetocentric because the pixels in the Cassini images were equally spaced in planetocentric coordinates. All other latitude offsets are planetographic. The last column gives the RMS value of the velocity over all latitudes. RMS values for HST 2008 and Cassini zonal velocities were found using CIV as described in Section 3.3. RMS values for the HST 1995–1998 and Voyager zonal velocities were found by taking the RMS value of the published RMS value at each latitude.

Data set	Latitude offset	Velocity offset (m s^{-1})	RMS velocity (m s^{-1})
HST 2008	0	0	11.2
Cassini 2000 (this paper)	0.12 (N) 0.02 (S)	−0.03 (N) 0.54 (S)	11.4
Cassini 2000 (Porco et al., 2003)	0.32 (N) 0.36 (S)	1.5 (N) 2.7 (S)	N/A
HST 1995–1998	−0.14	−7.2	8.0
Voyager 2	0.43	−2.5	6.4

4. Results using the global method

4.1. Comparison of HST 2008 and Cassini 2000 zonal velocities

Fig. 2a shows a plot of our HST 2008 and Cassini 2000 zonal velocities; the difference between these zonal velocities, along with the uncertainty in the difference are shown in panel b. The uncertainty in the difference at a given latitude is the composite uncertainty defined as $RMS_C \equiv \sqrt{(RMS_{Cassini2000})^2 + (RMS_{HST2008})^2}$. The uncertainties $RMS_{Cassini2000}$ and $RMS_{HST2008}$ are the RMS values of the *correlation velocity uncertainties*, as defined in Section 3.3, of the Cassini 2000 and HST 2008 zonal velocities, respectively. Differences greater than the uncertainty can be seen at eight different latitudes: 33.5°N, 31.1°N, 23.7°N, 8.2°N, 26.9°S, 29.9°S, 37.2°S and 47.8°S.

Local weather phenomena such as divergent motion from convective plumes, waves and vortices can cause errors in the zonal velocity measurements (García-Melendo and Sánchez-Lavega, 2001). It is partly for this reason that many previous studies have taken a time average of several zonal velocity measurements (Limaye, 1986, 1989; García-Melendo and Sánchez-Lavega, 2001; Porco et al., 2003). When constructing our Cassini 2000 zonal velocity, we used images from four jovian rotations, effectively allowing us to average three zonal velocities together. This reduced the likelihood that transient weather phenomena (with evolutionary timescales of less than four jovian days) would affect the zonal velocity. Our HST 2008 zonal velocity was more sensitive to short-timescale weather phenomena because it was constructed from data from only two jovian rotations. Weather that changes on longer timescales will have affected both data sets. One possibly reliable method for ferreting out spurious changes between the Cassini 2000 and HST 2008 zonal velocities would be to use an automated or manual cloud tracking method to find local motions near the latitude of interest at all longitudes, and use the resulting velocity field to detect weather phenomena. Unfortunately, this method is generally time consuming. Instead, we opted for a possibly less reliable but much faster method: we examined the cloud patterns in the mosaics directly, looking for signs of dominant vortex, wave or divergent motions at the latitudes of interest.

Fig. 3 shows close-up views of six regions from Fig. 1 covering all eight locations where changes in the zonal velocity may have occurred. Although it is not always correct to associate cloud patterns with streamlines of the flow, the wavy distortions in the clouds near 31°N in Fig. 3a suggest that there are significant north–south velocities at many longitudes along this latitudinal band, and that the possible change at this latitude is spurious. These wavy distortions extend north as far as 33.5°N, so we consider changes at this latitude also to be spurious. Fig. 3b shows no local weather features that would affect the zonal velocity measurement, so we conclude that the change at 23.7°N is real. Indeed, a change in the zonal velocity at this latitude, associated with the eruption of two convective plumes in March 2007, had been observed by Sánchez-Lavega et al. (2008) and Barrado-Izagirre et al. (2009), as we discuss in Section 4.5. Fig. 3c has a small, high contrast convective plume at 100°W, which could correspond to diverging fluid motion. Even given its high contrast, the plume's small size probably means it contributes negligibly to the zonal velocity at this latitude. Of greater concern are the dark projections at 8.2°N and their effects on the extracted velocities near them.

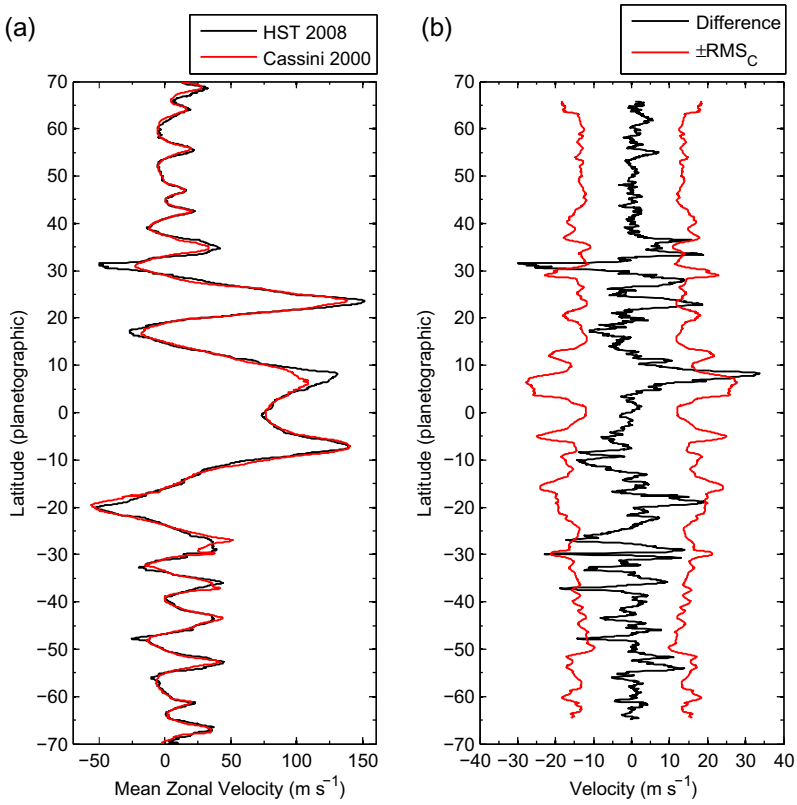

Fig. 2. (a) Our zonal velocity from HST images from May 10, 2008 and from Cassini images from December 11 to 13, 2000. The zonal velocities indicate a significant increase in the peak speeds of the zonal velocities near ∼33°N, ∼31.5°N, ∼23.7°N and ∼8°N latitude. Changes of more questionable significance can be seen at ∼26.5°S and ∼37.5°S latitude. (b) The difference between our HST our Cassini zonal velocities from (a). Also shown is the composite uncertainty of the two zonal velocities $\pm RMS_C \equiv \pm\sqrt{(RMS_{HST2008})^2 + (RMS_{Cassini2000})^2}$, where $RMS_{HST2008}$ and $RMS_{Cassini2000}$ are computed as in Section 3.3. Statistically significant changes occur only where the black curve lies outside the bounds of the shaded curves. Velocity increases at ∼33°N, ∼31.5°N, ∼23.7°N and ∼8°N latitude are all greater than the uncertainties, but the changes at ∼33°N and ∼31.5°N are likely to be spurious and due to waviness in the clouds. Changes at ∼26.5°S and ∼37.5°S latitude are only slightly larger than the uncertainties, and may or may not be significant. The change in velocity at ∼8°N is likely due to the fact that velocity-extraction algorithm used with the 2000 Cassini mistakenly found the drift velocities of the dark projections at that latitude, rather than the mean zonal velocity. See Section 5.

These features are thought to correspond to Rossby wave peaks and/or tied to elevations beneath the visible-cloud deck that move at speeds that differ from the zonal velocity of the visible-cloud deck. We defer the discussion of changes of the zonal velocity near 8°N to Section 5. Fig. 3d and e shows several vortices that may have introduced spurious changes at 26.9°S, 29.9°S and 37.2°S. Several patches that may correspond to cyclonic vortices occur near 47.8°S; two of these are faintly visible in Fig. 3f near 150–170°W and 60–90°W. A large number of small vortices are visible throughout this region. Both types of features could be interfering with the zonal velocity measurement, and hence we conclude that the change at 47.8°S may not be real. In either case, Fig. 2 shows that this change is only marginally greater than the uncertainties.

4.2. Comparison of HST 2008 and HST 1995–1998 zonal velocities

Most of the possible changes between 1995 and 2008 are similar to those between 2000 and 2008 (i.e., we see few differences between the HST 1995–1998 mean zonal velocity and the Cassini 2000 zonal velocity). Fig. 4a shows our HST 2008 zonal velocity and the HST 1995–1998 mean zonal velocity of García-Melendo and Sánchez-Lavega (2001), along with the difference and associated uncertainties (defined as in the previous section) between the zonal velocities in panel b. Statistically significant changes can be seen at seven latitudes: 31.1°N, 23.7°N, 7.7°N, 9.6°S, 18.2°S, 26.2°S and 54.1°S. (There are also several other locations where the magnitude of the possible changes are essentially equal to the uncertainties.) Five of these seven locations correspond to changes analyzed in the previous section; the remaining two changes at 9.6°S and 18.2°S most likely occurred between 1995 and 2000. The same analysis of the previous section applies to the five possible changes from after 2000: The change at 23.7°N is probably real; we defer the discussion about the changes at 7.7°N to Section 5. The change at 31.1°N is probably spurious (influenced by north–south fluid motion), as are the changes at 26.2°S and 54.1°S (due to vortex motion). Fig. 4 suggests that either there are remaining navigation errors between the HST 2008 and HST 1995–1998 zonal velocities in the southern hemisphere or that the locations of the east and west jets changed by as much as 1° latitude over the course of 10–13 years.

After García-Melendo and Sánchez-Lavega (2001) published their results, improved geometric distortion corrections were made available for WFPC2 (Anderson et al., 2003; Kozhurina-Platais et al., 2003). However, the improvement (on the order of 0.4 pixels for the WFPC2/PC1 detector) corresponds to an error of only about 0.1–0.2° latitude near disk center, increasing as $1/\cos(\theta)$ along the central meridian longitude (e.g., 0.25–0.3° latitude at 50°N). Additional errors may be associated with the variation in the distortion correction with wavelength, but it is unclear that the accumulation of errors in the distortion solution of individual frames could lead to the observed error of 1° at low latitudes.

4.3. Comparison of HST 2008 and Voyager 2 1979 zonal velocities

In this section, we compare our HST 2008 zonal velocity with the Voyager 2 mean zonal velocity of Limaye (1986). We do not

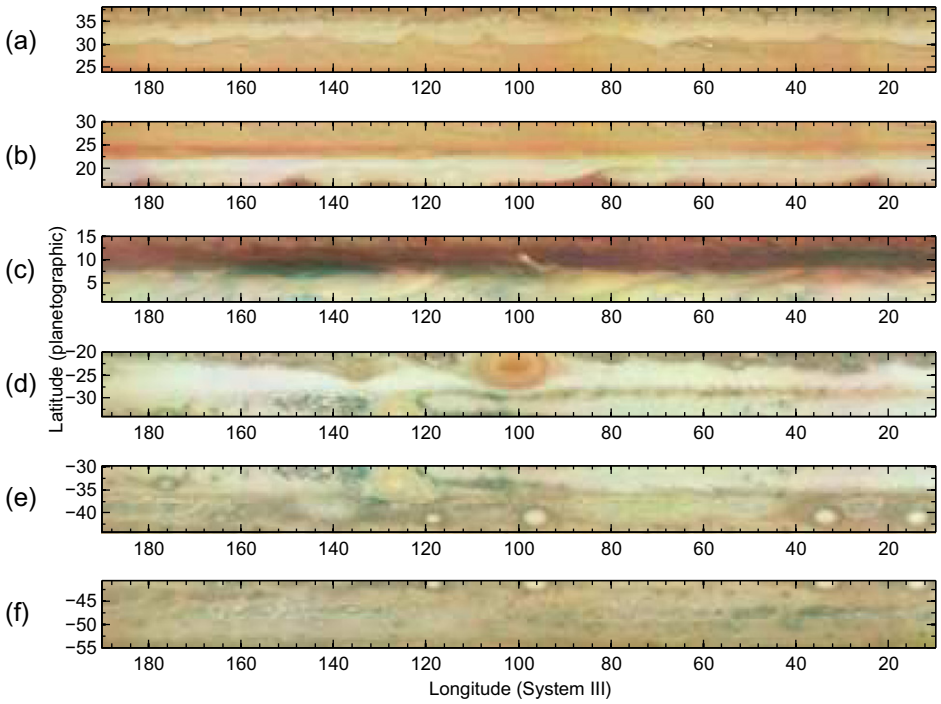

Fig. 3. Six parts of the HST mosaic in Fig. 1. The six regions are centered around the latitudes (a) ∼31.5°N, (b) ∼23.7°N, (c) ∼8°N, (d) ∼19°S, (e) ∼26.5°S and (f) ∼37.5°S, where Fig. 2 shows the largest changes in the zonal velocity between 2000 and 2008. (a) The wavy cloud patterns may correspond to significant north–south fluid motion, suggesting that velocities detected by our global method at 31.5°N and 33°N may not be real. (d)–(f) High contrast clouds associate with vortex features and turbulence near 19°S, 26.5°S and 37.5°S latitude may "confuse" the correlation algorithm, artificially modifying the measured zonal velocity. (b) and (c) Wave patterns, vortex features, dark projections and turbulence are *not* apparent at ∼23.7°N, suggesting that the correlation method is picking up the zonal fluid motion and that the changes in the zonal winds at these latitudes are real. The small convective plume near 100°W in (c) is probably too small to influence the zonal velocity measurement.

use the Voyager 1 mean zonal velocity published in Limaye (1989) because several factors make the latter Voyager zonal velocity less appealing for comparison than the former (fewer constituent zonal velocities used to compute the mean, the known latitudinal misnavigation and the use of images taken at multiple wavelengths). Fig. 5 shows ∼15 different locations where statistically significant changes are seen between 1979 and 2008. The locations of several jets have changed by as much as 1.5° latitude, and the peak velocities of several jets have changed by ∼10–15 m s^{-1}. The most significant possible changes are at 48.5°N, 7.8°N and 47.7°S. A comparison between Fig. 5 and the two panels in Fig. 4 suggests that the changes at 48.5°N and 47.7°S occurred between 1979 and 1998, while comparison with Fig. 2 suggests that the change at 7.8°N must have happened between 2000 and 2008 (but see Section 5).

4.4. Summary of significant changes between 1979 and 2008

Fig. 6a shows the difference between our HST 2008 zonal velocity and the other three zonal velocities—our Cassini 2000 zonal velocity (blue), the HST 1995–1998 zonal velocity (red) of García-Melendo and Sánchez-Lavega (2001) and the Voyager 2 1979 zonal velocity (black) of Limaye (1986). These three curves are the same as the black curves in Figs. 2b, 4b and 5b, respectively. Fig. 6b presents the same data in a slightly different fashion: The three curves show the change in the zonal velocity over three time periods – between 2000 and 2008 (blue), between 1995–1998 and 2000 (red), and between 1979 and 1995–1998 (black). Fig. 6 helps to synthesize the results of the previous three sections.

The major changes between 1979 and 1995–1998 have been discussed in detail in García-Melendo and Sánchez-Lavega (2001), and are summarized here for comparison with the other time periods. Changes can be seen in strength of many zonal jets, most notably those at ∼49°N and ∼24°N, which weakened by ∼30 m s^{-1}, and the jet near 48°S, which strengthened by ∼25 m s^{-1}. The broad velocity minimum near the equator decreased in speed by ∼20 m s^{-1}, while the eastward jet at 7°S strengthened by approximately the same amount (as observed by Vasavada et al. (1998), using images Galileo from November 1996). All jets poleward of 45°N and 45°S appear to have moved toward the equator by between 0.5° and 2° latitude during this time period. García-Melendo and Sánchez-Lavega (2001) attributed this trend to navigational errors; the fact that errors of this nature, and of this magnitude were not seen when comparing the other zonal velocities suggests either that the changes are real or that the errors lie predominantly in the navigation of the Voyager mosaics.

During the much shorter time interval between 1995–1998 and 2000, we see a few noteworthy possible changes as well. Two sharp spikes in our Cassini 2000 zonal velocity at 30°S and 37°S are probably spurious artifacts resulting from vortex motion in these regions; these sharp peaks were not seen in either the HST 1995–1998 or the HST 2008 zonal velocities. Long-lived, real changes of as much as 37 m s^{-1} appear to have occurred in the shearing region between 7°S and 20°S over these 2–5 years. García-Melendo and Sánchez-Lavega (2001) observed changes in the velocity in this region during the period between 1995 and 1998 that they averaged, so that it is difficult to say how much of the change occurred before 1998 and how much (if any) occurred after that year.

Although the differences in the zonal velocities indicate eight possible changes over the time period between 2000 and 2008, visual inspection of the mosaics suggests that six of these may be spurious. The remaining two changes, an ∼18 m s^{-1} velocity increase near 24°N, and a ∼34 m s^{-1} increase near 8°N, show no obvious signs of influence from local weather, though the Rossby waves may play a role in the observations at 8°N (see Section 5). Fig. 7a shows a

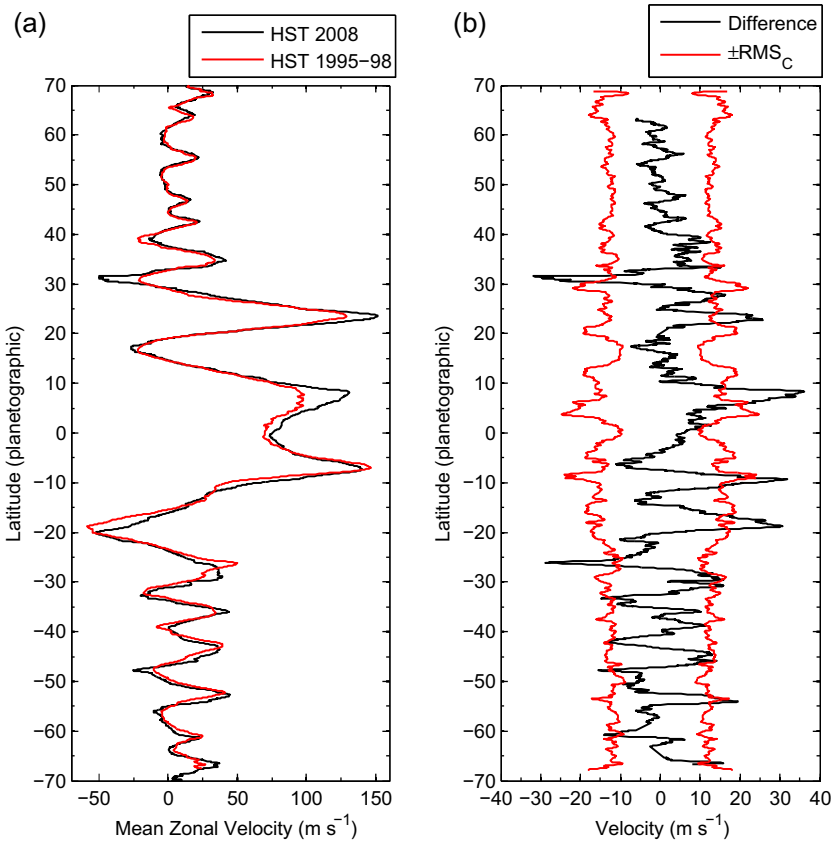

Fig. 4. (a) Our zonal velocity from HST images taken on May 10, 2008 and the zonal velocity of García-Melendo and Sánchez-Lavega (2001) from HST images taken between 1995 and 1998. The velocities indicate a significant increase in the peak zonal wind speed of three zonal jets, located at ~31.5°N, ~23.7°N, ~8°N, ~26.5°S and ~37.5°S latitude. (b) The difference between our HST zonal velocity and the HST zonal velocity of García-Melendo and Sánchez-Lavega (2001) from (a). Also shown is the composite uncertainty $\pm RMS_C \equiv \pm\sqrt{(RMS_{HST2008})^2 + (RMS_{HST95-98})^2}$ of the two zonal velocities. The velocity changes between 1995–1998 and 2008 at ~23.7°N and ~8°N latitude are statistically significant, whereas those near 31.5°N, 26.5°S and 37.5°S may be artifacts caused by waves and vortices at those latitudes. We believe that the velocity at ~8°N measured by García-Melendo and Sánchez-Lavega (2001) is likely to be incorrect due to spurious velocity correlations that come from the eastward drift of the dark projections at that latitude. See Section 5.

close-up view of all four zonal velocities (along with uncertainties) in the region near 24°N. The figure shows that the velocity at the peak decreased by ~30 m s^{-1} between 1979 and 1995–1998, but then regained much of its former strength between 2000 and 2008. Fig. 7b shows a similar plot of the region near 8°N. The peak in the eastward jet at this location is ~20 m s^{-1} stronger in 2008 than in any of the previous observations.

4.5. Observations near 24°N

Previous analyses of Jupiter's second strongest eastward jet, at 24°N, have identified this region as prone to zonal velocity changes. However, the timing and magnitude of the changes and the maximum zonal velocities in this jet are controversial. Maxworthy (1984) found a maximum velocity of ~180 m s^{-1} in 1979, ~20 m s^{-1} faster than Limaye (1986). It is unclear if this difference represents a real change (or variability) in the zonal velocity during the Voyager fly-bys or if the difference arises from the very different velocity-extraction methods that were used. Simon (1999) agreed with the previously noted decrease in maximum jet speed between 1979 and 1995, but found that the jet increased back to a maximum speed of 179 m s^{-1} in 1998. Using the *same* HST data, García-Melendo et al. (2000) and García-Melendo and Sánchez-Lavega (2001) instead found no change in the jet's maximum velocity between 1995 and 1998.

The 11 m s^{-1} increase in the maximum speed of the 24°N jet between 2000 and 2008 (Fig. 2) was not monotonic in time. Sánchez-Lavega et al. (2008) reported higher velocities of 160 m s^{-1} on 25 March 2007, coincident with the eruption of two highly energetic plumes at 23°N. Within about two months, the peak jet speed decreased to about 147 m s^{-1}, very close to the 2008 speed we report here. Both Simon (1999) and García-Melendo et al. (2000) reported a relationship between cloud patterns (morphology, color, and brightness) in the North Temperate Belt near this jet, although the direction of causality in this relationship is unconstrained by the data. The 2007 decrease in jet speed following the plume eruptions (Sánchez-Lavega et al., 2008) suggests an additional relationship between jet speed and release of internal heat. However, since the plumes traveled slightly faster than 160 m s^{-1}, it is not clear how they could have caused a decrease in the jet speed to 147 m s^{-1}. Understanding the physics relating the observations of jet speed, cloud patterns, and plume eruptions would advance our knowledge of Jupiter's internal heat release and of the remarkable stability of its zonal winds, but much higher temporal sampling of the zonal velocity field is needed to constrain the dynamics. Unfortunately, the need for high-resolution images to measure zonal winds requires the use of highly over-subscribed facilities such as the Hubble Space Telescope, making it unlikely that these mysteries will be solved in the near future.

Barrado-Izagirre et al. (2009) characterized the Fourier spectrum of the longitudinal spatial variability of cloud brightness at several wavelengths in the vicinity of 24°N. They also computed zonal velocities in this region with a manual cloud feature tracking method using images that, in most cases, covered ~125° longitude. Their zonal velocity measurements show an ~25 m s^{-1} increase in the speed of the westward jet at 17°N planetographic (15°N

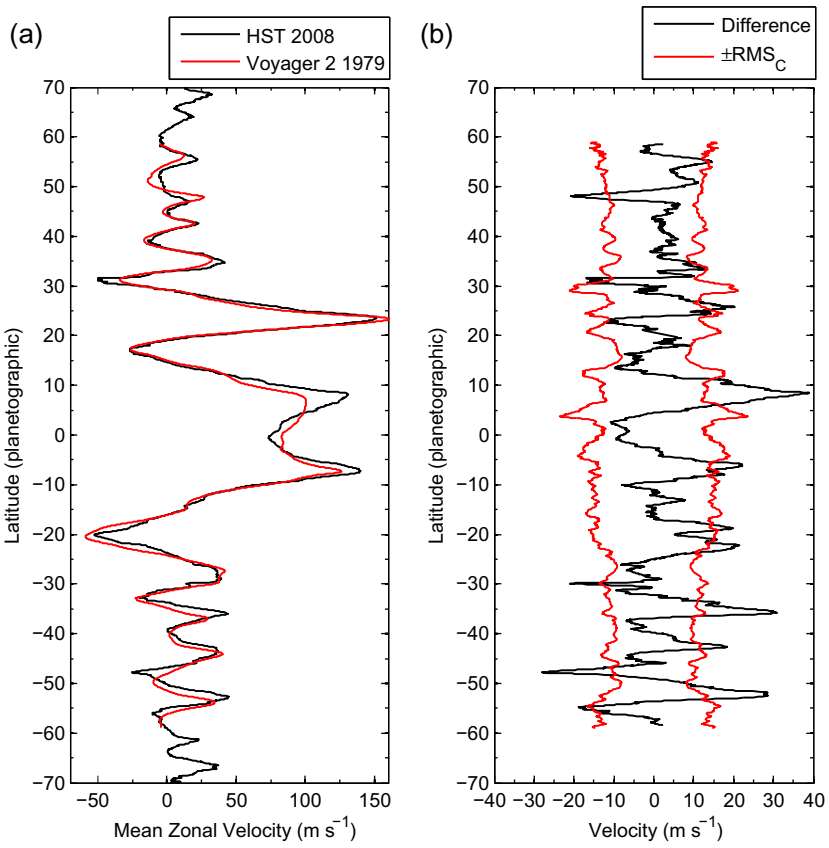

Fig. 5. (a) Zonal velocities from our HST images taken on May 10, 2008 and the Voyager 2 zonal velocity of Limaye (1986) from March 1979. We believe that the velocity at ~8°N measured by Limaye (1986) is likely to be incorrect due to spurious velocity correlations that come from the eastward drift of the dark projections at that latitude. See Section 5. (b) The difference between our HST zonal velocity and the Voyager 2 zonal velocity of Limaye (1986). Also shown is the composite uncertainty $\pm RMS_C \equiv \pm\sqrt{(RMS_{HST2008})^2 + (RMS_{Voyager2})^2}$.

planetocentric) latitude from ~15–25 m s^{-1} in March–June 2007 to ~50 m s^{-1} in July 2008. The peak velocity near 17°N from our May 2008 zonal velocity is ~27 m s^{-1}, consistent with the March–June 2007 measurements of Barrado-Izagirre et al. (2009), but not showing the increased speed they observed in July 2008. The differences may result from the incomplete longitudinal coverage in many of the zonal velocity measurements of Barrado-Izagirre et al. (2009), or from differences between our automated and their manual feature tracking methods. By matching their spectra and zonal velocities with those from EPIC simulations, Barrado-Izagirre et al. (2009) conclude that kinetic energy from the plume eruptions at 23°N was redistributed to the anticyclonic (equatorward) side of the eastward jet at this latitude, eventually producing a stronger westward zonal jet at 14°N. Given that we do not observe this change in the westward zonal velocity, our zonal velocity from May 2008 would appear to be inconsistent with their conclusion.

4.6. Method validation using Cassini images December 2000

To validate our global-velocity-extraction method, we compared our Cassini 2000 zonal velocity obtained via our global method with the Cassini 2000 zonal velocity produced by Porco et al. (2003). Both zonal velocities were produced from the same Cassini images (but with slightly different navigation and deprojection; Vasavada, A., personal communication). To compensate for some of the relative navigational differences, we shifted the Porco et al. (2003) zonal velocity relative to ours using the method described in Section 3.4. In the northern hemisphere, we found a best-fit planetocentric latitude offset of 0.32° and a velocity offset (at the equator) of 1.5 m s^{-1}; in the southern hemisphere, the best-fit planetocentric latitude offset was 0.36° and the velocity offset was 2.7 m s^{-1}. Fig. 8a shows a comparison of our Cassini 2000 zonal velocity with the zonal velocity of Porco et al. (2003); panel b shows the difference between the two zonal velocities along with $RMS_{Cassini2000}$ derived for our zonal velocity by the method of Section 3.3. The difference in the two zonal velocities is significantly less than $RMS_{Cassini2000}$ at all latitudes, and the RMS difference over all latitudes is 2.6 m s^{-1}. Our method seems to produce a reliable zonal velocity. (Porco et al. (2003) did not provide an uncertainty for their zonal velocity, so we used only our $RMS_{Cassini2000}$ when comparing the zonal velocities.)

The largest differences between the two globally-extracted Cassini zonal flows from 2000 are near 37°N and 30°S latitude. Fig. 9 shows image-strips of these regions, which both display substantial vortex activity. This activity may account for the differences in the zonal velocities.

5. Observations near 8°N

5.1. Concerns about the velocities of the dark projections

Our Cassini 2000 global-extraction of the zonal velocities near 8°N agrees with previously-published studies; the peak eastward flow is 108.8 m s^{-1}, consistent with the range of previously published values (for 1979–2000) that are between 103 and 114 m s^{-1} (Fig. 7b). However, the eastward drift speeds of the dark projections (which are associated with the 5 μm hot spots) near 8°N have also been measured, and they are between 97 and 116 m s^{-1} (Allison, 1990; Ortiz et al., 1998; Arregi et al., 2006). Because the dark projections are the highest contrast features near

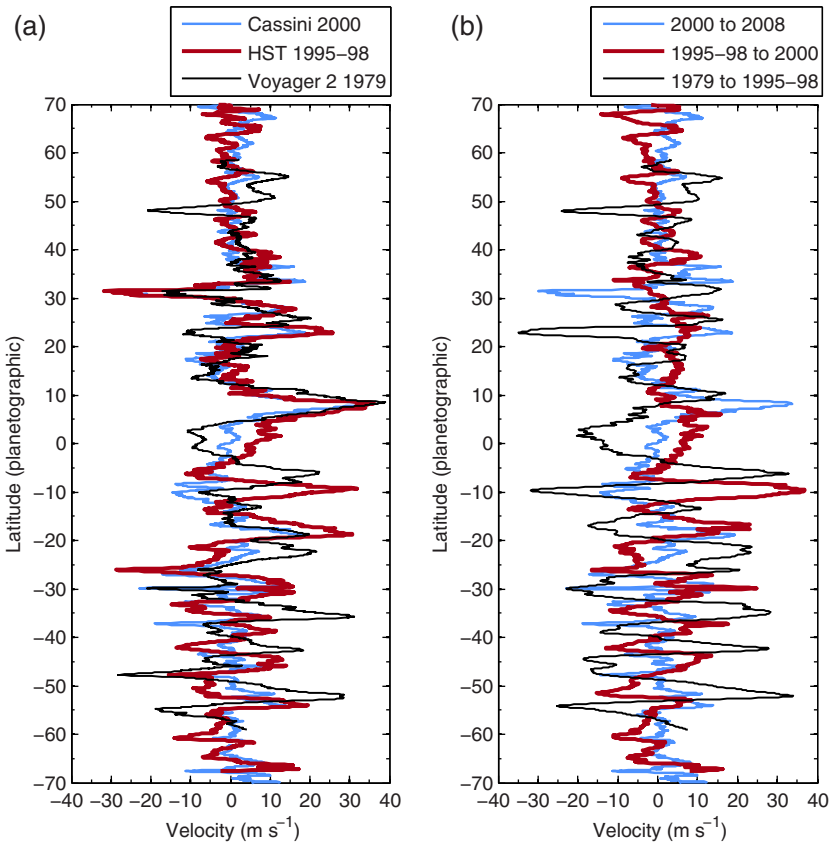

Fig. 6. (a) The difference between our HST 2008 zonal velocity and our Cassini 2000 zonal velocity (blue), the 1995-1998 HST zonal velocity of García-Melendo and Sánchez-Lavega (2001) (red), and the Voyager 2 zonal velocity of Limaye (1986) from 1979 (black). At three latitudes, ~31.5°N, ~8°N and ~26°S, we see noticeable changes in our HST 2008 zonal velocity where there was little variation in the three zonal velocities spanning 1979–2000. Analysis of the cloud features in Fig. 3 suggest that the northernmost and southernmost of these apparent changes are probably spurious. We believe that the ~30 m s^{-1} "increase" in the velocity of the eastward zonal peak near 8°N in 2008 is due to the fact that the 2008 measurement is of the actual zonal velocity at this latitude, whereas the other measurements were all "fooled" into finding the eastward drift velocities of the dark projections at this latitude. This figure also shows that the eastward jet near 24°N increased in velocity by ~20 m s^{-1} between 2000 and 2008, returning to the strength it had in 1979. (b) The difference between our HST 2008 zonal velocity and our Cassini 2000 zonal velocity (blue), between our Cassini 2000 and the HST zonal velocity of García-Melendo and Sánchez-Lavega (2001) from 1995–1998 (red), and between the HST 1995–1998 zonal velocity and the Voyager 2 zonal velocity of Limaye (1986) from 1979 (black). As discussed in Section 4.4, changes in the zonal velocity can be seen at a variety of locations during these three periods of time. (For interpretation of the references to color in this figure legend, the reader is referred to the web version of this article.)

8°N at visible wavelengths used to compute zonal velocities, it is plausible that our global method, as well previous methods of zonal velocity extraction, are fooled into finding the drift rates of the dark projections rather than the true zonal velocity at these latitudes.[3]

Another potential problem at 8°N is that the peak zonal velocity found there with our globally-extraction method using the HST 2008 images is ~131.2 m s^{-1}. Thus, if our 2000 and 2008 zonal velocities are correct, then the velocity peak at 8°N increased by 22 m s^{-1} between 2000 and 2008, which is larger than any other change in the zonal velocity between 2000 and 2008. (The second largest change was at 31.1°N, but was likely spurious as discussed in Section 4.1.) Such a large increase in zonal velocity should be viewed with caution, and may suggest that either the 2000 or 2008 (or both) velocity measurements near 8°N were incorrect. It would be useful to know if the eastward drift speed of the dark projections in 2008 was also ~131 m s^{-1}, which might explain the increase in our "extracted" (but possibly incorrect) zonal velocity. Arregi et al. (2006) catalogued drift rates of the dark projections between 1882 and 2001, showing that they always lie in the range of 97–114 m s^{-1}, making a drift rate of over 130 m s^{-1} very unlikely. Unfortunately, no drift rate measurements have been made since 2001, so we cannot be certain (but see Section 5.3).

5.2. Zonal velocities extracted by the local method

The velocities and cloud patterns in the region around 8°N have large variations in longitude. By extracting two-dimensional velocity vectors from the Voyager data with manual methods, Ingersoll et al. (1981) and Limaye et al. (1982) found an unusually large RMS deviation of the zonal velocity measurements of ~20 m s^{-1} in this region. Unlike previously-published automated methods that were used to compute zonal velocities, these manually extracted velocity vectors were able to capture the longitudinal variability of the zonal velocity. This variability may be due to waves (see next section), or due to longitudinally varying cloud opacities that allow us to observe deeper into the atmosphere. With longitudinally varying cloud opacity, vertical wind shear could account for the measured longitudinal variation in the extracted velocities. Li et al.

[3] There are high-contrast vortex streets at other latitudes, and the vortices drift east and west with respect to the ambient zonal flows, so why do not the velocity-extraction algorithms get fooled at these latitudes as well? It appears that sometimes they do. However, the vortices drift independently of each other and do not cover a wide range of longitudes, so that when their east–west velocities are averaged in longitude and/or time, the spurious velocities of the vortices average to zero with respect to the local zonal velocity. In contrast, all of the clouds patterns of the 8–10 dark projections drift at nearly the same speed with respect to their local zonal flow, so their spurious effects do not average to zero as they do in a row of independently drifting vortices.

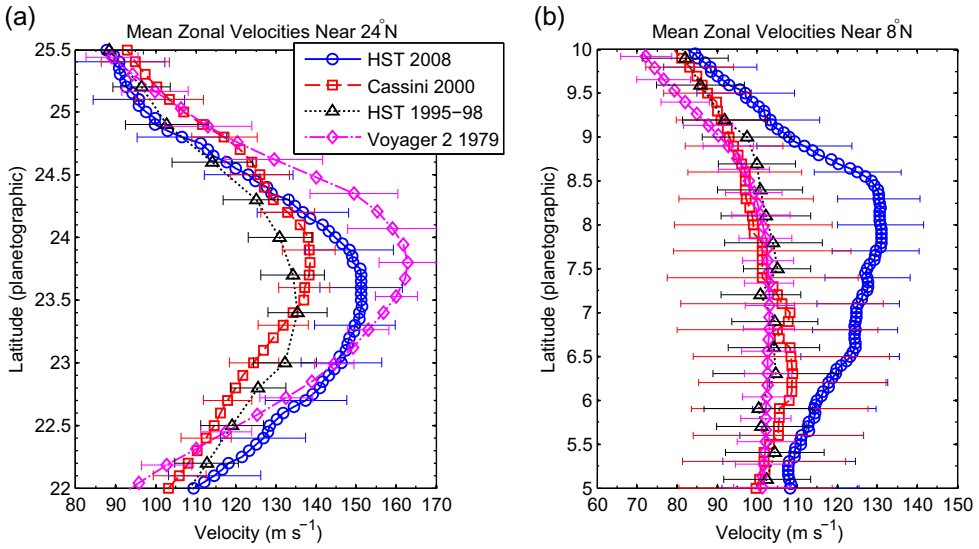

Fig. 7. (a) The four zonal velocities near 24°N: Our HST 2008 zonal velocity (blue circles), our Cassini 2000 zonal velocity (red squares), the HST zonal velocity of García-Melendo and Sánchez-Lavega (2001) from between 1995 and 1998 (black triangles), and the Voyager 1 zonal velocity of Limaye (1986) from 1979 (magenta diamonds). The velocity magnitude of the eastward jet in 2008 is ~15 m s^{-1} greater than in both 2000 and 1995–1998, but ~10 m s^{-1} less than in 1979. The error bars shown in the plot are $RMS_{HST2008}$, $RMS_{Cassini2000}$, $RMS_{HST95-98}$ and $RMS_{Voyager2}$ as defined in the text. The error bars indicate that the changes between 1995–2000 and 2008 are greater than the uncertainties. (b) The four zonal velocities and RMS uncertainties near 8°N plotted as in (a). The velocity magnitude of the eastward jet in 2008 is ~30 m s^{-1} greater than seen in the three earlier zonal velocities. The error bars indicate that the change between 1979–2000 and 2008 is greater than the uncertainty but is misleading if the velocity-extraction algorithms are being "fooled" by the drift velocities of the dark projections. (For interpretation of the references to color in this figure legend, the reader is referred to the web version of this article.)

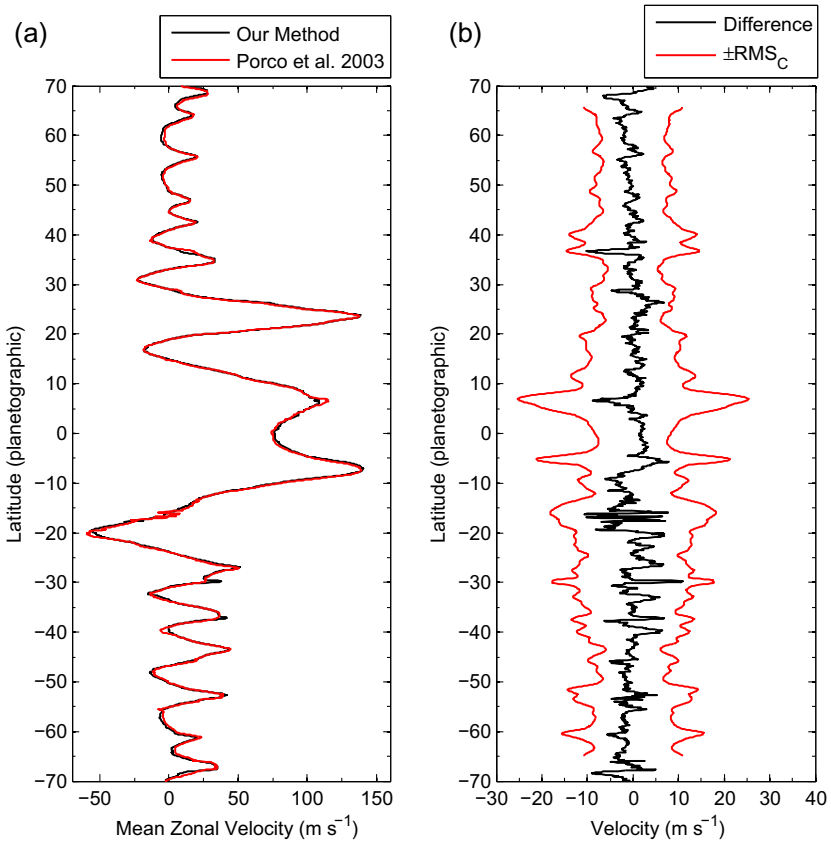

Fig. 8. (a) Our zonal velocities from Cassini images taken on December 11–13, 2000 and the zonal velocity of Porco et al. (2003) from Cassini images from the same dates. The zonal velocities are similar at most locations. (b) The difference between our Cassini zonal velocity and the Cassini zonal velocity of Porco et al. (2003). Also shown is $RMS_{Cassini2000}$ as a function of planetographic latitude. All differences are smaller than the RMS uncertainties.

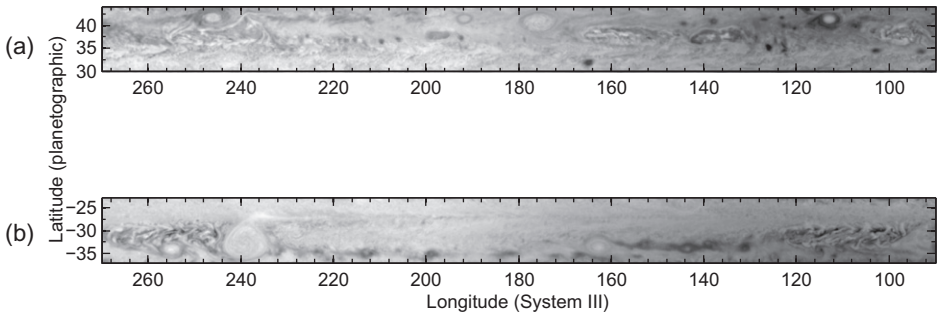

Fig. 9. Two parts of a Cassini mosaic taken at 750 nm (CB2 filter) on December 11, 2000. The two regions are centered around the locations of maximum difference between our Cassini 2000 zonal velocity an the Cassini zonal velocity of Porco et al. (2003) at (a) ∼37°N and (b) ∼30°S latitude (see Fig. 8). Both regions contain vortical features with high contrast clouds that probably dominated the comparisons made by our correlation method, leading to small errors in the zonal velocity.

(2006) and Atkinson et al. (1998) both argued that there is a large vertical zonal wind shear at 8°N. Li et al. (2006) based their arguments on velocities extracted from Cassini images taken at several wavelengths and by peering through the "holes" in the visible-cloud deck provided by the dark projections. Atkinson et al. (1998) measured the zonal velocity near the 3-bar height from Doppler velocity measurements with the Galileo probe. This combination of vertical zonal wind shear and longitudinally varying cloud opacity could account for the longitudinal variability in the extracted zonal velocity vectors at this latitude.

To untangle these issues we developed a *local* method for extracting the zonal velocity that allows us to better understand the longitudinal variability of the zonal velocity. By applying Advection Corrected Correlation Image Velocimetry (ACCIV), the automated velocity extraction technique described in Asay-Davis et al. (2009), to the same Cassini 2000 images that we used to compute our *globally*-extracted Cassini 2000 zonal velocity, we have derived the two-dimensional velocity map of the full planet between ±60°. The longitudinally-averaged, east–west component of this velocity map is defined to be our *locally*-extracted zonal flow and is shown in Fig. 10a. The difference between the locally- and globally-derived zonal velocities using the Cassini 2000 data is shown in Fig. 10b. The difference is small at most latitudes, but there is a large difference near 8°N. (The other big differences are near 31.1°N, which we have discussed in Sections 4.1 and 4.2 as a region of waviness in the visible clouds and 29.9°S, where vortex motion probably are responsible for the spurious spike in the velocity.) Fig. 10b shows that the difference between the locally- and globally-extracted zonal velocities at this latitude is approximately the same as the RMS value of the correlation uncertainty.

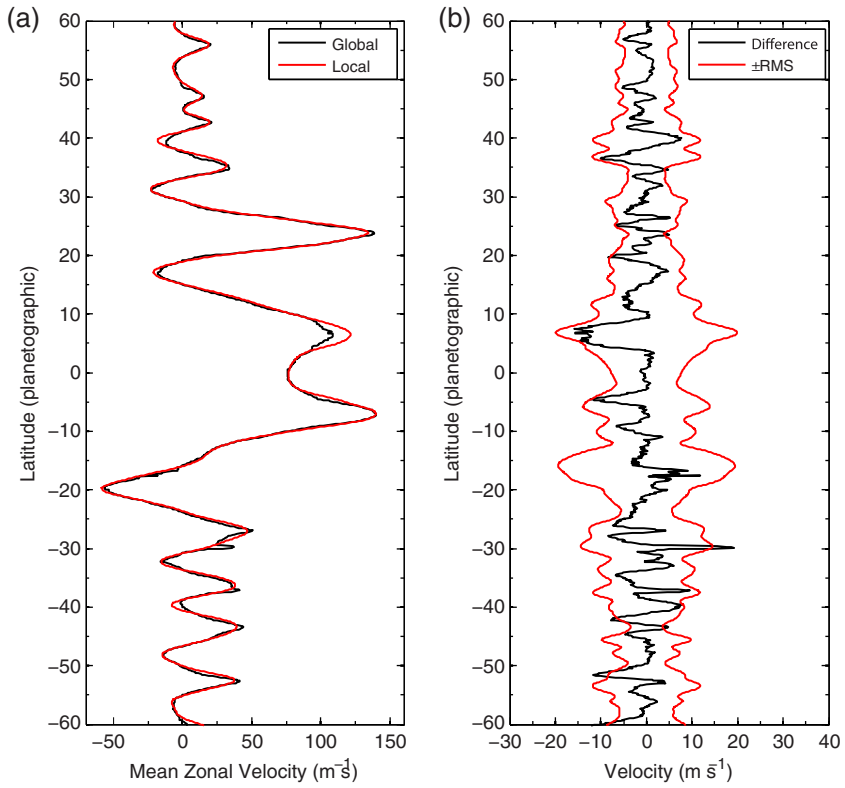

Fig. 10. (a) The Cassini 2000 zonal velocity extracted with the *local correlation technique* from Section 5.2 and extracted with the *global correlation technique* from Section 3.2. The zonal velocities agree at most latitudes but show a few marked differences, notably at 8°N. (b) The difference between the two zonal velocities from (a) along with the RMS uncertainties. The uncertainties show unusually large variability in the jet at 8°N as well as in the shear region between 7°S and 20°S. The fact that the difference curve lies close to the left RMS uncertainty curve in the region near 8°N indicates that the global correlation technique is systematically finding the smallest magnitude velocities at these latitudes. Fig. 11 shows that the smallest speeds are well correlated with the dark cloud features of the dark projections.

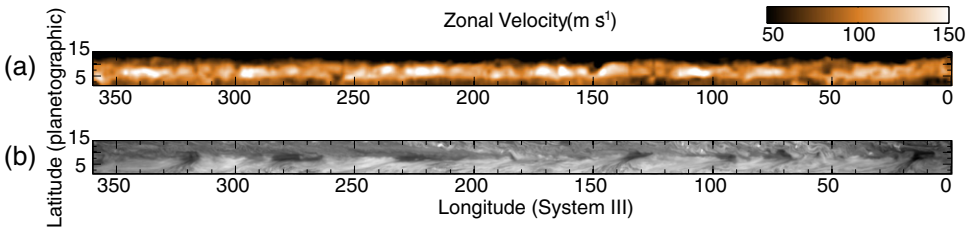

Fig. 11. (a) A map showing the spatial variability of the east–west component of the velocity based on Cassini 2000 images taken at visible wavelengths. The information in the map was derived from the *two-dimensional* velocity field that we extracted from the images using ACCIV (Asay-Davis et al., 2009) for latitudes between 60°N and 60°S and for all longitudes. Near 8°N the east–west component of the velocity varies from ~100 to 150 m s^{-1} as a function of longitude. (b) A mosaic made from Cassini images showing the same region as (a). Visual comparison shows that the regions of lowest velocity in (a) (darker shades of orange) are usually well correlated with the location of the seven dark projections, which are the dark features centered at longitudes 13°, 72°, 94°, 133°, 225°, 275°, and 320°. Although the regions inside the dark projections are nearly free of visible clouds, with ACCIV we have extracted ~100,000 two-dimensional velocity vectors within the dark projections. Not much information can be inferred about those velocity vectors, it is not clear what heights in the atmosphere those velocities correspond to, or if the velocities are associated with the internal dynamics of the dark projection or the ambient zonal flow. Those velocity vectors trace local dynamics related to the dark projections, rather than the drift velocity of the dark projections. (For interpretation of the references to color in this figure legend, the reader is referred to the web version of this article.)

The two coincide because both of these quantities primarily measure the longitudinal variation in the east–west velocity. The longitudinal variation of the magnitude of the east–west component of the velocity near 8°N is illustrated by the color-map in Fig. 11a. Comparison between this panel and Fig. 11b shows that six of the seven dark projections are located at longitudes where the east–west velocity has its lowest values, ~100 m s^{-1}.

Fig. 12 illustrates another new way to see that the east–west components of the two-dimensional velocities extracted from the images in visible wavelengths depend on whether they are inside or outside of the dark projections. The figure not only compares the zonal velocities extracted with the local method and with the global method but also shows the average east–west components (as functions of latitude) of the two-dimensional velocity vectors within each of the seven dark projections. Note that one of the dark projection (at longitude 225°) has fluid with in it that has velocities with east–west components that are faster than the locally-extracted velocity (which at each latitude bin is the average of the east–west component of the two-dimensional velocity field averaged over all longitudes, except for the parts of the velocity field that lie within any one of the seven dark projections). Note that the average of the east–west component of the two-dimensional velocity vectors within a dark projection is *not* the speed at which the dark projection drifts to the east, so visible clouds trace local and zonal motions but do *not* trace the propagation of equatorially trapped Rossby waves.

Ideally, we would apply the same ACCIV velocity-extraction method to the HST images from May 2008 in order to create a velocity map near 8°N similar to Fig. 11. Based upon our findings when we applied ACCIV to regions on these images near GRS and Red Oval, the signal to noise ratio of these images is too low to apply ACCIV in a reliable way. However, because the local-velocity-extraction method and the global-velocity-extraction method when applied to the Cassini 2000 images yield nearly the same zonal velocities (with the exception of 29.9°S, which is likely spurious due to vortices and 8°N due to dark projections), and because the vector fields that are used to compute the locally-extracted zonal velocity (with the exceptions of 29.9°S and 8°N) do not show much longitudinal variation, we believe that longitudinal variation of cloud opacity (except at 8°N) does not lead to spurious results.

5.3. Analysis of the flow at 8°N

From the discussion in the previous section and from Figs. 10–12, we conclude that our global-extraction method using the Cassini 2000 images taken at visible wavelengths did *not* find the mean zonal velocity at the level of the visible clouds at 8°N. Fig. 11a shows that the east–west component of the velocity near 8°N has significant variations in longitude and that large regions of the flow near that latitude have east–west velocity components of order 140 m s^{-1}.

Li et al. (2006) argued that the dark projections act as windows in the visible clouds and allow the CB2 and MT2 filters to pick up high-speed (typically, ~150 m s^{-1}) velocity vectors at elevations *beneath* the visible clouds. Our ACCIV velocity-extraction method with images in visible wavelengths is able to find correlations between image pairs of clouds (and thereby extract velocities) within the relatively cloud-free dark projections (cf., Fig. 13). However, Figs. 12 and 13 show that the velocities that we extracted from within the dark projections are generally (i.e., six out of seven cases) slower than the velocities that we found outside the dark projections, and those velocities are always very much smaller than the high-speed velocities (140–175 m s^{-1}) found by Li et al. (2006). Note that with our automated method we have found ~100,000 velocity vectors within the dark projections, whereas Li et al., who used a manual method to find correlations, report only 15 velocity vectors within the dark projection that they examined (at 225 longitude) and approximately one-third of those vectors had velocities less than 115 m s^{-1}. It is possible that the high-speed velocities that Li et al. report come from a deep (>3 bar) layer of fast zonal flow, but, based on Figs. 11–13, we believe an equally plausible explanation is that: (1) all or most of the velocity vectors that we have extracted from the visible-wavelength images outside the dark projections are at the visible-cloud level; (2) the zonal flow at 8°N has a peak eastward velocity of 122–140 m s^{-1}; and (3) the velocity vectors we obtain within the dark projections are at visible-cloud level or deeper, but they are associated with the complex fluid dynamics and cloud patterns within the dark projections rather than the zonal velocity either at the visible-cloud level or at the 3-bar level.[4] Because we do not thoroughly understand the dynamics of the dark projections (or their precise relationship to the 5 μm hot spots) and in particular how the winds within them are structured or whether their clouds are passive tracers, we believe that we should simply exclude their contribution (as we have done in the dashed curve in Fig. 12) from the averaging used to compute the zonal flow at visible-cloud level (or at a deeper level).

The fact that both Porco et al. (2003) and we found peak velocities at 8°N, of ~111 m s^{-1} using global velocity-extraction methods on the Cassini 2000 images, means that these methods are *not* finding the average zonal velocity at the visible-cloud level,

[4] Velocity measurements in the regions of dark projections (Hueso and Sánchez-Lavega, 1998; Vasavada et al., 1998) tracked features around and exterior to the dark projections rather than within them.

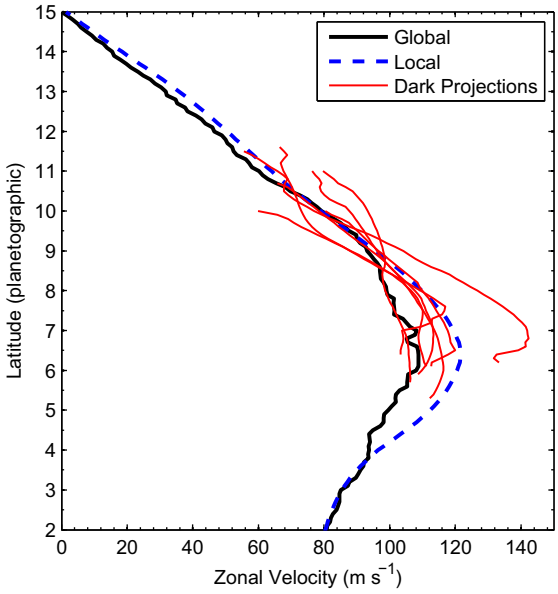

Fig. 12. Details of the globally- and locally-extracted zonal velocities shown in Fig. 10a. Also shown are the averaged east–west components (as functions of latitude) of the two-dimensional velocity vectors within each of the seven dark projections (associated with the 5 μm hot spots). For each of the red curves and for each latitude bin, to compute the zonal flow we carried out the averaging over longitudes that are within 0.5° (in all directions) of the dark patches thought to indicate the dark projection. Six of the seven dark projections have averaged east–west velocities that are less than the zonal velocity as determined by the local method. Note that the averaged east–west velocities within each of the seven dark projections are very different, despite the fact all seven dark projections have nearly the same eastward drift velocity. The red curve with the largest peak eastward-going velocity (142.3 m s^{-1}) is for the dark projection at 220° longitude and is the same dark Projection that was used in the study by Li et al. (2006) who found 15 velocity vectors within the dark projection, with the biggest velocity vector having an east–west component of 175 m s^{-1}. (For interpretation of the references to color in this figure legend, the reader is referred to the web version of this article.)

nor are they finding the characteristic east–west velocity components outside the dark projections. Thus, it appears that these global methods, as well as *all* previous studies using visible images from 2000 or earlier (which *all* found peak velocities of ∼103–114 m s^{-1} near 8°N) failed to find the zonal velocity, and instead found the drift velocity of the dark projections (which therefore cannot be passively moving at the visible-cloud level east–west velocities).

The one exception where it appears that a global-velocity-extraction method using images taken at visible wavelengths does *not* find drift the velocity of the dark projections is our global-velocity extraction using the 2008 HST images. That analysis found a peak velocity of 131.2 m s^{-1}, and it is difficult to believe that that was the drift velocity of the dark projections in 2008. Unfortunately we do not know their drift speed in 2008 (nor do we have a 2D east–west velocity field for 2008), but we can put bounds on the drift speeds of the dark projections in 2008 if they move at the phase speed of a Rossby wave, as suggested by Allison (1990), Ortiz et al. (1998), Arregi et al. (2006). The only parameters that affect the speed of a Rossby wave and that can change in time are: its azimuthal wavenumber (i.e., the number of dark projections), the vertical stratification (parameterized as the equivalent height by Allison (1990)), the velocity of the underlying zonal flow to which the Rossby wave is attached, and the Rossby wave's meridional wavenumber. Ortiz et al. (1998) and others have argued that the meridional wavenumber must be unity in order to have the Rossby wave have a large amplitude near 8°N. The number of dark projections has either remained the same or has decreased by one between 2000 and 2008 (see Figs. 3c and 11b – we suggest that there are six dark projections in 2008, but the imagery is not definitive; it is generally agreed that there were seven in 2000), but the phase speed of a Rossby wave *decreases* with a decreasing number of dark projections (azimuthal wavenumber). The number of dark projections would have had to increase from 7 to 26 between 2000 and 2008 for the speed of the Rossby wave and of the dark projections to have increased from 108.8 to 131.2 m s^{-1}. Or, if the number of dark projections had stayed the same (i.e., 7) between 2000 and 2008, the equivalent vertical depth of the layer containing the wave (as defined by Allison (1990)) would have had to have changed from 0.9 km (Ortiz et al., 1998) to a very shallow 210 m between 2000 and 2008 to obtain a similar increase in the Rossby wave phase speed. Such a large change in equivalent depth would have had many other observational consequences. Of course, if the velocity of the underlying zonal flow to which the Rossby wave is attached increased by 22 m s^{-1}, it would cause an increase in the Rossby wave speed from 109 to 131 m s^{-1}, but we consider that explanation not to be very likely.

A more plausible explanation is that the eastward drift speed of the dark projections in 2008 was still between 97 and 116 m s^{-1} and that our global-velocity-extraction algorithm applied to the HST 2008 data found an average (over most longitudes, including the regions of the dark projections which generally have anomalously small east–west velocity fields within them) of the zonal

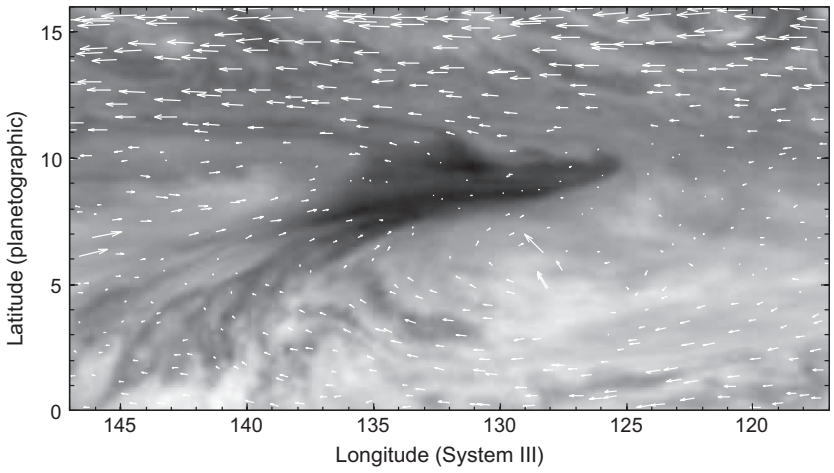

Fig. 13. The clouds and extracted two-dimensional velocity vectors from one of the dark projections shown in Fig. 11b. For clarity, we have shown only one out of every 256 extracted velocity vectors (i.e., 1/16 in each dimension). The magnitudes of the largest vectors (along the top of the figure) are approximately 100 m s^{-1}. We subtracted an eastward velocity of 100 m s^{-1} from all vectors, so that the velocities are in a frame approximately translating with the dark projection.

velocity near 8°N. This is plausible because a comparison of Fig. 3c and Fig. 11b shows that the dark projections' features have lower contrast in the HST 2008 images than they do in the Cassini 2000 images, and therefore the dark projections have less effect on the velocity extraction technique when applied to the HST 2008 images. Thus, we conclude that our best estimates for the zonal flow near 8°N are the *local* measurements in 2000 (Fig. 10a) and the global measurements in 2008 (Fig. 2), which both show peak velocities of $\sim$127 m s^{-1}, in contrast to the dark projection drift speeds of 97–116 m s^{-1}. However, it should be kept in mind that Fig. 11a shows that there is a great deal of longitudinal variation at this latitude and that the regions within the dark projections have a much slower east–west velocity. Therefore, a more representative estimate of the zonal peak velocity near 8°N might be as high as 140 m s^{-1}.

6. Conclusions and future work

6.1. Physics of the zonal flows

As in earlier studies of the zonal flows of Jupiter at the visible-cloud level, we have found that Jupiter's zonal flows are robust. In particular, in most cases the maxima of the eastward- and westward-going jet streams moved by less than ±1° latitude (but more than the observational uncertainty) between 1979 and 2008. The caveat to this observation is that there appear to be relative navigational errors in latitude among the different data sets that were used in this study — see the next subsection.

All of the previous studies of the zonal velocity near 8°, as well as our velocity-extraction from the Cassini 2000 images with the global method, appear to be erroneous because they find the eastward drift speed ($\sim$100 m s^{-1}) of the dark projections rather than the true zonal velocity.

Local velocity-extraction methods using ACCIV on the Cassini 2000 images in visible wavelengths indicate that the zonal velocity has a large longitudinal variability due to the dark projections but that the average zonal velocity is $\sim$130 m s^{-1}. Therefore, we disagree with the conclusions of Vasavada et al. (1998) and Li et al. (2006) that the dark projections (or 5 μm hot spots) move at the same speed at their local zonal flow. The dark projections drift eastward slower than their ambient visible-cloud-level zonal velocity. A zonal velocity of $\sim$130 m s^{-1} agrees (within observational uncertainties) with our globally-extracted zonal velocity from the HST 2008 images (which were not strongly affected by the dark projections because their cloud features had less contrast in 2008 than they had previously).

All studies of the jovian zonal flows have shown a double-pronged equatorial zonal wind that was characterized by strong eastward-going jets at ±7°, but the jets are asymmetric with the northern jet much weaker than the southern. If the previous results at 7°N are discounted due to the errors from the dark projections and if the zonal velocity at 7°N in those studies is replaced either by our globally-extracted velocity using the HST 2008 data or our locally-extracted velocity using the Cassini 2000 data, then the two jets become nearly symmetric about the equator (cf., Figs. 4a and 5a).

The zonal flow at the 3-bar height and 7.3°N was measured by the Galileo probe to be $\sim$170 m s^{-1}. If the zonal wind velocity at that latitude and at the visible-cloud level is $\sim$130 m s^{-1} and therefore larger than previously reported, then the vertical zonal wind shear will be smaller than the currently accepted value. In addition, we find that the east–west flow velocity at visible-cloud level, near 7°N, and at longitudes between the dark projections is $\sim$140 m s^{-1}. If this latter velocity is used as the characteristic zonal velocity at visible-cloud level near 7°N, then the vertical zonal wind shear between the visible-cloud level and the 3-bar is less than half the currently accepted value.

Consistent with the analyses of Limaye (1986, 1989) and García-Melendo and Sánchez-Lavega (2001), we find long-term fluctuations in the magnitudes of the zonal velocities that are of order 10–20 m s^{-1}. García-Melendo and Sánchez-Lavega (2001) found variations of this magnitude in their zonal velocities covering the time period between 1995 and 1998, and the zonal velocities presented in Section 4 show variations on this scale during all time periods we examined: 1979 to 1995–1998, 1995–1998 to 2000, and 2000 to 2008. If the correlation uncertainty of the zonal velocity represents real fluctuations, rather than observational errors, then the zonal fluctuations could be due to temporal fluctuations that occur on timescales less than 10 h, indicating that there are fluctuations of order 10 m s^{-1} on scales ranging from hours to years. However, it is also possible that the correlation uncertainty of the zonal velocity is not due to temporal fluctuations, but rather due to fluctuations of the zonal velocity as a function of longitude, or departures of the *direction* of the zonal velocity at some longitudes from the east–west direction. Determining the source of the correlation is possible by examining the extracted velocity fields as in Asay-Davis et al. (2009), rather than an extracted zonal velocity, but is beyond the scope of the present study and part of our future work. If, as suggested by the correlation uncertainty of 11 m s^{-1}, there are spatial fluctuations of the zonal velocity of order 10%, or temporal fluctuations during a 10-h period of order 10%, there may be serious consequences for previous studies that have assumed that there are no fluctuations in the zonal flow. Studies of the mergers and interactions of jovian vortices are not likely to be affected. However, our own study of vortex/zone interactions (Shetty and Marcus, 2010) had to be modified after we realized that the zonal flow had fluctuations of 10%. Other calculations, such as those that compute the transfer of angular momentum between the Great Red Spot and its surrounding zonal flow, may also require serious modification (Salyk et al., 2006). The velocity fluctuations pose both interesting challenges and benchmarks for those who model Jupiter's zonal flows.

Although there is no obvious natural velocity in Jupiter's weather layer that would imprint the value of 10–11 m s^{-1} on the fluctuations, we can easily translate between velocity scales and length scales. Jupiter's zonal flows have characteristic peak shears $\sigma \simeq 10^{-5}$ s^{-1} (Shetty and Marcus, 2010). In a shear flow, cross-stream spatial fluctuations of length scale λ produce velocity fluctuations of order $\sigma\lambda$, so velocity fluctuations of 11 m s^{-1} are readily produced by spatial fluctuations of order 1000 km, which is of order the Rossby deformation radius. Thus, small vortices or waves could produce fluctuations of order 10–11 m s^{-1}. Most theoretical models of Jupiter's zonal flows fall into two categories: self-organization, via turbulent inverse energy cascade of the small-scale flows in a shallow layer system; or the large scale response of vertical motions in a convectively forced deep-layer system (Sayanagi et al., 2008; Vasavada et al., 2005). In the former, fluctuations would be expected on the scale of the deformation radius via inverse cascades. In the latter, one might expect the imprint of the deformation radius on the large scale flow because the deformation radius is a function of the vertical stratification. In any case, we have shown that there are correlation fluctuations and changes in the jovian zonal velocity of $\sim$10 m s^{-1} on temporal scales ranging from hours to decades, while the latitudinal locations of the velocity extrema of the zonal jets remain fixed. Therefore, a test of the accuracy of future theoretical or computational studies of the Jupiter's zonal flows, especially those that use global circulation models, is that they reproduce these fluctuations while maintaining the constancy of the latitudinal locations of the zonal velocity extrema.

6.2. Velocity extraction methodology

We showed that velocities extracted from images taken with different visible wavelengths (but at different times) produce similar zonal velocities, supporting the conclusions of others that the velocities all come from the same visible-cloud level. This result for Jupiter appears to be in contrast to the results for Saturn (Porco et al., 2005). Jovian horizontal velocities might also be extracted from tracers at deeper levels within the dark projections at 8°N. However, regardless of what elevation those velocities come from, velocities extracted from regions within the dark projections will contaminate the computation of mean zonal flow because those velocities are likely to be indicative of the dynamics of the dark projections themselves.

Comparing velocity changes (either over time or among different research groups) requires better image navigation than is being currently done. In particular, we have claimed that in most cases the maxima of the eastward- and westward-going jet streams moved by less than ±1° latitude (but more than the observational uncertainty) between 1979 and 2008. However, the caveat to this observation is that there appear to be relative navigational errors in latitude among the different data sets that were used in our study. Without making corrections for navigational errors, the velocity peaks among the different data sets are misaligned by up to ∼0.5° latitude. We believe that a significant portion of the misalignment of velocity peaks is due to navigational errors rather than a real shift in latitude of the winds, because a single north–south shift between each data sets improves the alignment of *all* of 29 of the velocity peaks (spanning ±70° latitude), rather than just making a single peak align.

We have shown that our local method for computing zonal velocities, in which the two-dimensional velocity field is found (with ACCIV) prior to averaging its east–west component over longitude, does not get "fooled" into finding the drift rates of the dark projections instead of the actual zonal velocity. The local method also provides a direct measure of the longitudinal fluctuations of the velocity and a determination of how large the meridional velocity components are compared to the east–west components. Ideally, we would apply the local method to all of our images. However, the signal to noise ratio of HST/WFPC2 2008 images may be too low to allow for the production of reliable velocity maps; this was our finding when we applied ACCIV to the regions of these images near GRS and Red Oval. In addition, it is very time consuming to compute velocities that cover large portions of the planet. The Cassini 2000 velocity map between ±60° and over all longitudes, part of which we used to compute the local-velocity extraction in Section 5.2, took more than a month to compute on a four processor desktop computer. The high computational cost and sensitivity to noise, together with the fact that the resulting mean zonal velocity (see Fig. 10a) is smoother in latitude more than the global correlation result, suggest that full velocity maps are not yet ready to replace global-velocity-extracting methods. When possible, it seems preferable to compare mean zonal velocities produced by both techniques. In this way, regions of agreement and low longitudinal variability can be distinguished from more suspect regions of disagreement and/or high longitudinal variability. When it is not possible to compute a reliable 2D velocity map (as with our May 2008 HST images), it is important that the results of global correlation methods be viewed with caution, and that efforts be made to identify, and perhaps mask out, meteorological phenomena (waves, vortices, etc.) that can lead to spurious mean velocity measurements.

The mean zonal velocities and their uncertainties reported here for 1979 and for 1995–1998 were determined by other authors. Those zonal velocities were computed from the unweighted arithmetic averages of N samples taken at nearby, but different, times; the uncertainties were found by computing the RMS differences among the zonal velocities. Limaye (1986, 1989) reported the uncertainties of the zonal velocity based on the RMS values of the differences divided by $\sqrt{N}$, consistent with the assumption that the differences among the zonal velocities were random. If on the other hand, as the data suggest, there are variations of the zonal flow that are coherent over timescales that are of the order of the window of time in which the samples are collected, the RMS values themselves are more meaningful measures of the uncertainties. In our calculations of the uncertainties of the zonal velocities in 2000 and in 2008, each uncertainty was computed from a single zonal velocity extracted from a pair of images that span ∼10 h. Our uncertainties were based on the RMS value of the *correlation uncertainty* over a large subset of all of the correlations in an image pair. For both the 2000 and 2008 zonal velocities, we found an uncertainty of ∼11 m s^{-1}. It is curious that the uncertainties based on our correlation analyses over 10-h periods are approximately the same as the magnitude of the fluctuations that Limaye (1986, 1989) and García-Melendo and Sánchez-Lavega (2001) found over weeks, months, years, and decades. We argue that the uncertainty that we found based on correlations is not due to observational errors and represents real fluctuations of the velocity. One reason for our argument is that the Cassini 2000 data set that we used in determining the zonal velocity in 2000 was the same data set that we used to computed the velocity fields of the Great Red Spot and Oval BA. For those velocity fields we found that the RMS correlation uncertainties were 7 m s^{-1} and 6.5 m s^{-1}, respectively (Asay-Davis et al., 2009), suggesting that the observational errors are less than or equal to 6.5 m s^{-1}, which in turn suggests that the zonal velocity correlation uncertainty of 11 m s^{-1} is due at least in part to real fluctuations.

Our global-velocity-extraction method using the HST 2008 data appears to have worked near 8°N and not been "fooled" into finding the eastward drift speeds of the dark projections. However, to confirm this result it would be useful to determine the drift speed values in 2008 directly from archived and amateur images. In addition, because amateur images taken as this article goes to press (late 2010) show very low contrast between dark projections and their surroundings, it would be useful to obtain current HST images pairs so that the zonal velocity could be computed by both the local- and global-extraction methods without any contamination from the dark projections.

Acknowledgments

The 2008 HST observations were obtained under HST program 11102, with support provided by NASA through a grant from the Space Telescope Science Institute, which is operated by the Association of Universities for Research in Astronomy, Inc., under NASA Contract NAS 5-26555. Analysis was supported by grants from the Planetary Atmospheres Program of NASA and the Astronomy and Astrophysics Program of NSF, with a computational allocation from the TeraGrid funded by NSF.

Appendix A. Image identifiers

The image identifiers for the images used to produce the HST 2008 zonal velocity were: ua0n0101m, ua0n0102m, ua0nb103m, ua0nb104m, ua0na101m, ua0na105m, ua0n0201m, ua0n0202m, ua0nb203m, ua0nb206m, ua0nb207m, ua0n0301m, ua0n0302m, ua0nb303m, ua0nb304m, ua0nc301m, ua0nc302m, ua0n0501m, ua0n0502m, ua0nb503m, ua0nb504m, ua0na501m, ua0na505m, ua0n0701m, ua0n0702m, ua0nb703m, ua0nb704m, ua0na701m, ua0na705m, ua0n0901m, ua0n0902m, ua0nb901m, ua0nb902m, ua0nc901m, ua0nc902m, ua0n1001m, ua0n1002m, ua0na001m,

ua0na005m, ua0nb003m, ua0nb004m, ua0n1101m, ua0n1102m, ua0nd103m, ua0nd104m, ua0nc101m and ua0nc105m.

The image identifiers for the Cassini-2000 zonal velocity were: n1355233441.1, n1355233845.1, n1355237227.1, n1355237631.1, n1355241013.1, n1355241417.1, n1355245203.1, n1355248585.1, n1355248989.1, n1355252371.1, n1355252775.1, n1355256157.1, n1355256561.1, n1355259943.1, n1355260347.1, n1355263729.1, n1355264133.1, n1355267515.1, n1355267919.1, n1355271301.1, n1355271705.1, n1355275087.1, n1355275491.1, n1355278873.1, n1355279277.1, n1355282659.1, n1355283063.1, n1355286445.1, n1355286849.1, n1355290231.1, n1355290635.1, n1355294017.1, n1355294421.1, n1355297803.1, n1355298207.1, n1355301589.1, n1355301993.1, n1355305375.1, n1355305779.1, n1355309161.1, n1355309565.1, n1355312947.1, n1355313351.1, n1355316733.1, n1355317137.1, n1355320519.1, n1355320923.1, n1355324305.1, n1355324709.1, n1355328091.1, n1355328495.1, n1355331877.1, n1355332281.1, n1355335663.1, n1355336067.1, n1355339449.1, n1355339853.1, n1355343235.1, n1355343639.1, n1355347105.1, n1355347598.1, n1355350891.1, n1355351384.3, n1355354677.1, n1355355143.1, n1355358463.1, n1355358929.1, n1355362211.1, n1355362570.1, n1355365978.1, n1355366357.1, n1355369821.1, n1355370295.1, n1355373607.1 and n1355374081.1.

References

Allison, M., 1990. Planetary waves in Jupiter's equatorial atmosphere. Icarus 83, 282–307.

Anderson, J., King, I.R., 2003. An improved distortion solution for the Hubble Space Telescope's WFPC2. Publ. Astron. Soc. Pacific 115, 113–131.

Arregi, J., Rojas, J.F., Sánchez-Lavega, A., Morgado, A., 2006. Phase dispersion relation of the 5-micron hot spot wave from a long-term study of Jupiter in the visible. J. Geophys. Res. (Planets) 111, 9010.

Asay-Davis, X.S., Marcus, P.S., Wong, M.H., de Pater, I., 2009. Jupiter's shrinking Great Red Spot and steady Oval BA: Velocity measurements with the 'Advection Corrected Correlation Image Velocimetry' automated cloud-tracking method. Icarus 203, 164–188.

Atkinson, D.H., Pollack, J.B., Seiff, A., 1998. The Galileo probe Doppler wind experiment: Measurement of the deep zonal winds on Jupiter. J. Geophys. Res. 103, 22911–22928.

Barrado-Izagirre, N., Pérez-Hoyos, S., García-Melendo, E., Sánchez-Lavega, A., 2009. Evolution of the cloud field and wind structure of Jupiter's highest speed jet during a huge disturbance. Astron. Astrophys. 507, 513–522.

Fincham, A., Delerce, G., 2000. Advanced optimization of correlation imaging velocimetry algorithms. Exp. Fluids 29, S013–S022.

Fincham, A.M., Spedding, G.R., 1997. Low cost, high resolution dpiv for measurement of turbulent fluid flow. Exp. Fluids 23, 449–462.

Flasar, F.M. et al., 2004. An intense stratospheric jet on Jupiter. Nature 427, 132–135.

García-Melendo, E., Sánchez-Lavega, A., 2001. A study of the stability of jovian zonal winds from HST images: 1995–2000. Icarus 152, 316–330.

García-Melendo, E., Sánchez-Lavega, A., Gómez, J.M., Lecacheux, J., Colas, F., Miyazaki, I., Parker, D., 2000. Long-lived vortices and profile changes in the 23.7°N high-speed jovian jet. Icarus 146, 514–524.

Higgins, C.A., Carr, T.D., Reyes, F., 2007. A new determination of Jupiter's radio rotation period. In: Rucker, H.O., Bauer, S.J., Lecacheux, A. (Eds.), Proceedings of the 4th International Workshop on Planetary Radio Emissions IV Held at Graz, Austria, September 9–11, 1996. Austrian Academy of Sciences Press, Vienna, pp. 43–50.

Hueso, R., Sánchez-Lavega, A., 1998. Motions in jovian hot spot plume regions using Voyager images. Icarus 136, 353–357.

Ingersoll, A.P., Beebe, R.F., Mitchell, J.L., Garneau, G.W., Yagi, G.M., Muller, J.-P., 1981. Interaction of eddies and mean zonal flow on Jupiter as inferred from Voyager 1 and 2 images. J. Geophys. Res. 86, 8733–8743.

Kozhurina-Platais, V., Anderson, J., Koekemoer, A.M., 2003. Toward a Multi-Wavelength Geometric Distortion Solution for WFPC2. Space Telescope Science Institute, WFPC2 Instrument Science Report 2003-02.

Li, L., Ingersoll, A.P., Vasavada, A.R., Porco, C.C., Del Genio, A.D., Ewald, S.P., 2004. Life cycles of spots on Jupiter from Cassini images. Icarus 172, 9–23.

Li, L., Ingersoll, A.P., Vasavada, A.R., Simon-Miller, A.A., Del Genio, A.D., Ewald, S.P., Porco, C.C., West, R.A., 2006. Vertical wind shear on Jupiter from Cassini images. J. Geophys. Res. (Planets) 111 (E10), 4004.

Lii, P., Wong, M., de Pater, I., 2010. Temporal variation of the troposheric cloud and haze in the jovian equatorial zone. Icarus 209, 591–601.

Limaye, S.S., 1986. Jupiter: New estimates of the mean zonal flow at the cloud level. Icarus 65, 335–352.

Limaye, S.S., 1989. Jupiter: Short-term variations of the mean zonal flow at the cloud level. NASA Special Publ. 494, 311–323.

Limaye, S.S., Revercomb, H.E., Sromovsky, L.A., Krauss, R.J., Santek, D.A., Suomi, V.E., 1982. Jovian winds from Voyager 2. I – Zonal mean circulation. J. Atmos. Sci. 39, 1413–1432.

Limaye, S.S., Sromovsky, L.A., 1991. Winds of Neptune: Voyager observations of cloud motions. J. Geophys. Res. 96, 18941–18960.

Martin, S.C., de Pater, I., Gibbard, S.G., Marcus, P., Roe, H.G., Macintosh, B.A., Max, C.E., 2004. Adaptive optics imaging of small cloud features on Neptune: Zonal wind variability and detections of oscillations in longitude. Bulletin of the American Astronomical Society, vol. 36. Bulletin of the American Astronomical Society, p. 1073.

Maxworthy, T., 1984. The dynamics of a high-speed jovian jet. Planet. Space Sci. 32, 1053–1055.

Ortiz, J.L., Orton, G.S., Friedson, A.J., Stewart, S.T., Fisher, B.M., Spencer, J.R., 1998. Evolution and persistence of 5-μm hot spots at the Galileo probe entry latitude. J. Geophys. Res. 103, 23051–23069.

Pearson, F., 1990. Map Projections: Theory and Applications. CRC Press, Boca Raton, FL.

Porco, C.C. et al., 2005. Cassini imaging science: Initial results on Saturn's atmosphere. Science 307, 1243–1247.

Porco, C.C. et al., 2003. Cassini imaging of Jupiter's atmosphere, satellites, and rings. Science 299, 1541–1547.

Russell, C.T., Yu, Z.J., Kivelson, M.G., 2001. The rotation period of Jupiter. Geophys. Res. Lett. 28, 1911–1912.

Salyk, C., Ingersoll, A.P., Lorre, J., Vasavada, A., Del Genio, A.D., 2006. Interaction between eddies and mean flow in Jupiter's atmosphere: Analysis of Cassini imaging data. Icarus 185, 430–442.

Sánchez-Lavega, A. et al., 2008. Depth of a strong jovian jet from a planetary-scale disturbance driven by storms. Nature 451, 437–440.

Sayanagi, K.M., Showman, A.P., Dowling, T.E., 2008. The emergence of multiple robust zonal jets from freely evolving, three-dimensional stratified geostrophic turbulence with applications to Jupiter. Icarus 65, 3947–3962.

Seidelmann, P.K. et al., 2007. Report of the IAU/IAG working group on cartographic coordinates and rotational elements: 2006. Celest. Mech. Dynam. Astron. 98, 155–180.

Shetty, S., Marcus, P.S., 2010. Changes in Jupiter's Great Red Spot (1979–2006) and Oval BA (2000–2006). Icarus 210, 182–201.

Simon, A.A., 1999. The structure and temporal stability of Jupiter's zonal winds: A study of the north tropical region. Icarus 141, 29–39.

Smith, B.A., Soderblom, L.A., Banfield, D., Barnet, C., Beebe, R.F., Bazilevskii, A.T., Bollinger, K., Boyce, J.M., Briggs, G.A., Brahic, A., 1989. Voyager 2 at Neptune – Imaging science results. Science 246, 1422–1449.

Vasavada, A.R., Horst, S.M., Kennedy, M.R., Ingersoll, A.P., Porco, C.C., Genio, A.D.D., West, R.A., 2006. Cassini imaging of Saturn: Southern-hemisphere winds and vortices. J. Geophys. Res. 111, E05004.

Vasavada, A.R., Showman, A.P., 2005. Jovian atmospheric dynamics: An update after Galileo and Cassini. Rep. Prog. Phys. 68, 1935–1996.

Vasavada, A.V. et al., 1998. Galileo imaging of Jupiter's atmosphere: The Great Red Spot, equatorial region, and White Ovals. Icarus 135, 265–275.